



Predicting the impacts of land use/land cover changes on seasonal urban thermal characteristics using machine learning algorithms

Abdulla - Al Kafy^{a,b,1}, Milan Saha^{c,d,1}, Abdullah-Al- Faisal^{a,e}, Zullyadini A. Rahaman^{f,*}, Muhammad Tauhidur Rahman^g, Desheng Liu^h, Md. Abdul Fattahⁱ, Abdullah Al Rakib^a, Ahmad E. AlDousari^j, Sk Nafiz Rahaman^k, Md Zakaria Hasan^l, Md Ahsanul Karim Ahsan^m

^a Department of Urban & Regional Planning, Rajshahi University of Engineering & Technology (RUET), Rajshahi, 6204, Bangladesh

^b ICLEI – Local Governments for Sustainability, South Asia, Dhaka, Bangladesh

^c Department of Urban & Regional Planning, Bangladesh University of Engineering & Technology (BUET), Dhaka, Bangladesh

^d School of Environmental Science and Management, Independent University of Bangladesh, Bangladesh

^e Department of Applied Geographical Information Systems and Remote Sensing, University of Southampton, SO17 1BJ, Southampton, United Kingdom

^f Department of Geography & Environment, Faculty of Human Sciences, Sultan Idris Education University, Tanjung Malim, 35900, Malaysia

^g Department of City and Regional Planning, King Fahd University of Petroleum & Minerals, KFUPM Box 5053, Dhahran, 31261, Saudi Arabia

^h Department of Geography, Ohio State University, Columbus, OH, United States

ⁱ Department of Urban and Regional Planning, Khulna University of Engineering and Technology, Khulna, Bangladesh

^j Department of Geography, Kuwait University, Kuwait City, Kuwait

^k Urban and Rural Planning Discipline, Khulna University, Khulna, 9208, Bangladesh

^l Department of Geography & Environmental Studies, University of Chittagong, Bangladesh

^m Department of Computer Science, Dalhousie University, Canada

ARTICLE INFO

Keywords:

Land cover change
Thermal comfort
Urban heat island
Machine learning algorithms
Prediction

ABSTRACT

Changes in land use/land cover (LULC) and land surface temperatures (LST) contribute significantly to the formation and intensity of urban heat islands (UHI) effects. The urban thermal field variance index (UTFVI) can effectively describe any city's UHI (thermal characteristics) effect. This study aims to assess and predict the seasonal (summer and winter) UTFVI scenario to evaluate the thermal characteristics of Sylhet city, Bangladesh. Landsat 4–5 TM and 8 OLI images from 1995 to 2020 were used to assess the previous status of LULC and UTFVI and predict the future changes for 2025 and 2030 using cellular automata and artificial neural network machine learning algorithms. Prediction results indicate a substantial increase in urban built-up areas by 42% and 44% in 2025 and 2035, followed by reductions in green cover (21% and 22%), bare land (20% and 21%) and water bodies (1%). The rapid expansion of built-up areas will lead to 13 km² and 14 km² stronger UTFVI zones in the predicted years. The study provides effective strategies for mitigating the UTFVI effects by avoiding dense infrastructural development, increasing plantation and water bodies, rooftop gardening and using white colour roofs in construction. The findings of this study will allow the urban planners, policymakers and local government to ensure an eco-friendly, inclusive and sustainable urban development through functional modification and replacement of the LULC distribution depending on the present and future circumstances.

1. Introduction

Cities are the engine of development. The climatic condition of cities is the most critical environmental factor impacting thermal

characteristics, ecosystem services and day-to-day activities. In addition, climate change deteriorates environmental sustainability by unpredictable weather patterns, reducing rainfall, declining water resources, intense droughts and urban flooding. Unplanned transformation in

* Corresponding author. Department of Geography & Environment, Faculty of Human Sciences, Sultan Idris Education University, Malaysia.

E-mail addresses: abdulla-al.kafy@localpathways.org (A.A. Kafy), milansaha023@gmail.com (M. Saha), abdullah-al-faisal@localpathways.org (A.-A. Faisal), zully@fsk.upsi.edu.my (Z.A. Rahaman), mtr@kfupm.edu.sa (M.T. Rahman), liu.738@osu.edu (D. Liu), mafattah.kuet@gmail.com (Md.A. Fattah), abdullahalrakib310@gmail.com (A. Al Rakib), dr.dousari@ku.edu.kw (A.E. AlDousari), sknafizrahaman1@gmail.com (S.N. Rahaman), zakariahasan062@gmail.com (M.Z. Hasan), ahasan.karim47@gmail.com (M.A.K. Ahsan).

¹ The authors contributed equally.

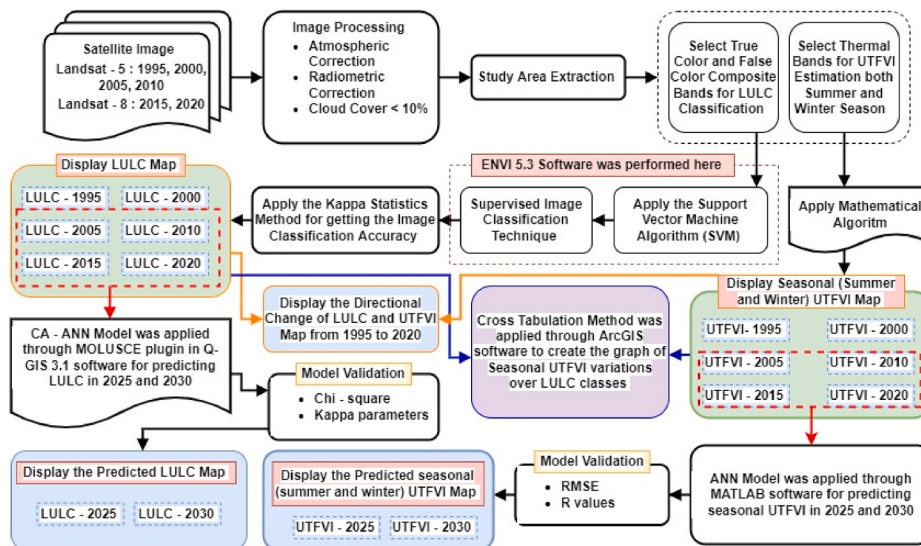


Fig. 1. Flow chart of detail methodological process for this study.

cities' land use/land cover (LULC) accelerates climate change by reducing agricultural land, green cover and water resources, which has severe impacts on food security, land surface temperature (LST) and urban heat island (UHI) [1]. Rapid urbanization and high-scale rural to urban migration contribute to intensifying the residential, commercial and utility needs and demands in urban areas. These results in large-scale LULC changes, such as converting forest, vegetation, and agriculture lands into built-up areas, resulting in the rapid increase of urban impervious surfaces [2]. Hence, eco-friendly LULC types, forest coverages, and natural water resources are shrinking daily and escalating the urban thermal effects [3–5]. Aside from the close association between changes in impervious surfaces and population growth, several socioeconomic and political factors have also influenced urbanization and changes in landscape patterns [4].

Unplanned urbanization and LULC changes have many detrimental repercussions, including urban sprawl development, increasing land values, poor sanitation, inadequate road networkings, insufficient water supplies, and reduction of vegetation lands [6]. It also declines the city's sustainability and increases environmental vulnerability to national and global climate change [7]. In particular, cities in Bangladesh have witnessed massive LULC transformation in recent decades and contribute to the thermal environment by formulating UHI effects [8,9]. Thus, understanding the influences of historical LULC change on the city scale is of great interest in the context of local and global warming.

Remote sensing (RS) and Geographic Information Systems (GIS) technologies can provide advanced support for effective monitoring of the spatiotemporal LULC changes, ecological conditions, and thermal patterns at the local, regional, and global scales [10]. Remotely sensed Landsat satellite images for earth observation are useful data sources for classifying the LULC and LST of the earth's surfaces [1]. Landsat data are frequently used for fair spatial and temporal resolutions, historical archiving, and global coverage availability [11,12]. The images are frequently classified using the maximum likelihood supervised classification method [1,13,14]. Urban Thermal Field Variance Index (UTFVI) is one of the most effective indices for monitoring the ecological conditions and identifying the city's heat stress scenario [3]. The effectiveness of UTFVI for assessing thermal characteristics of cities has been explained in several recent articles [15]. According to Dissanayake et al. [13], surface temperature represents the thermal characteristics and is positively correlated with the density of impervious surfaces and is sensitive to increased surface temperature. The concentration of UTFVI is more in cities than surrounding suburban areas due to more built-up areas. In addition, thermal characteristics of the built-up area are more

sensitive to increase temperature and UHI effects than any type of land use [14]. The UTFVI accelerates the thermal intensity of UHI that causes negative impacts on city's wind pattern, air quality, humidity, diurnal temperate range, phenology of vegetation, water consumption, indirect economic loss, reduced living comfort, the likelihood of heatwaves and mortality rate [16–21]. According to Im et al. [22], the South Asian agricultural region may see intense heatwave conditions in the future due to the increase in built-up areas. Ensuring the city's sustainability by controlling the impacts of thermal characteristics considering economic development is a major challenge, and assessing this phenomenon has been gaining great interest in the last few decades.

The UTFVI values are inversely related to the thermal comfort of a region. Values near zero represent the thermal condition best for the living environment, whereas increasing values of UTFVI represent the most vulnerable environmental conditions [9]. Due to unplanned urbanization, the areas with the worst thermal conditions have increased over the decades. In contrast, areas with tolerable thermal conditions are shrinking annually [23–25]. Besides, the intensity of the UTFVI phenomenon contributes to more heat zone in the major cities of Bangladesh. Thus, proper land use planning, promoting the plantation program, and using less energy-consuming materials, can be applied to reduce the UTFVI effect and improve the ecological condition of cities [10].

Over the last decade, machine learning (ML) algorithms have gained popularity in the classification of satellite data, including random forest (RF), support vector machine (SVM), and fuzzy ARTMAP, with each having various degrees of accuracy levels. Researchers have found that RF and SVM classify images with very high accuracy levels (more than 80%) [26]. Hence, they are the most frequently used technique among all ML classification techniques [26–28]. The assessment and prediction of LULC patterns can help city planners and policymakers to predict the likelihood of future urban growth and take the necessary precautions to make the city less vulnerable to climate change. Cellular Automata (CA) algorithm was applied for predicting the future LULC in Semarang and Cumilla correspondingly [10,29]. Further, the Artificial Neural Network (ANN) model was implemented to predict the future seasonal (summer and winter) UTFVI for 2030 in Dhaka City [9].

Although UTFVI varies between cities, existing research shows that human development-oriented LULC changes, with augmented anthropogenic activities, are primarily responsible for producing excessive heat in urban neighbourhoods. Therefore, location-specific assessments and measures are required. Monitoring and prediction related studies for LULC change are traditional approaches in GIS and RS perspectives.

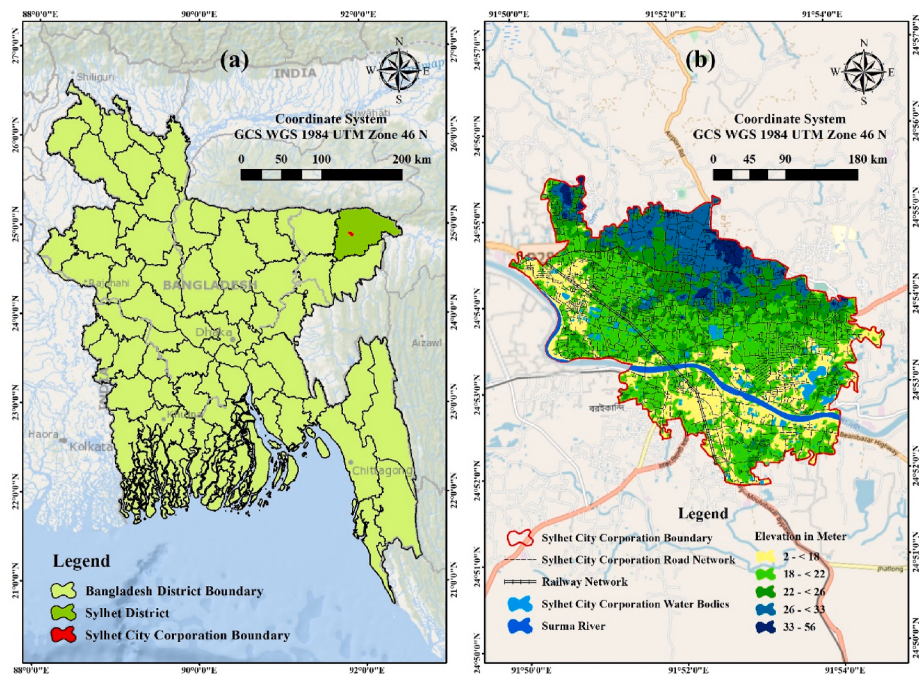


Fig. 2. Location map of the study area a) SCC in Bangladesh b) SCC.

Table 1
Description of the seasonal Landsat datasets downloaded from USGS.

Season	Date Acquired (Y/M/D)	Scene ID	Sensor	Cloud Cover	Path/Row
Summer Season (March to June)	1995/03/19	LT51360431995078ISP00	Landsat 4-5 TM	<10%	136/43
	2000/04/04	LT51360432000094BKT01		<10%	
	2005/05/01	LT51360432005121BKT00		<10%	
	2010/05/15	LT51360432010135KHC00		<10%	
	2015/03/10	LC81360432015069LGN01	Landsat 8 OLI	<10%	136/43
	2020/05/10	LC81360432020131LGN00		<10%	
Winter Season (December to February)	1995/01/30	LT51360431995030BKT00	Landsat 4-5 TM	<10%	136/43
	2000/02/29	LT51360432000060BKT00		<10%	
	2005/02/10	LT51360432005041BKT00		<10%	
	2010/01/23	LT51360432010023KHC00		<10%	
	2015/01/02	LC81360432015002LGN01	Landsat 8 OLI	<10%	136/43
	2020/01/19	LC81360432020019LGN00		<10%	

However, assessing and predicting the impacts of LULC on UTFVI is a relatively new concept and has only been addressed by a few studies. No study previously investigated the spatio-temporal and future impacts of LULC change on thermal characteristics (UTFVI) in Sylhet City Corporation (SCC). Identification of city-scale warming patterns and LULC change might help decision-making and support the emerging “smart city” concept, which aims to promote sustainable urban growth. The findings and recommendations provided in this study may also be helpful in designing location-specific adaptation strategies to mitigate environmental consequences and improve urban people’s quality of life. The objectives of this study are -

- Explore the LULC and seasonal UTFVI patterns from 1995 to 2020,
- Assess micro-scale directional changes of LULC and UTFVI in the last 25 years
- Estimate seasonal UTFVI variations over different LULC classes from 1995 to 2020
- Predict future LULC and seasonal UTFVI scenarios using machine learning algorithms for 2025 and 2030.

2. Materials and methods

This section will briefly discuss the methods used in this study. The detailed methodological process to achieve the objectives of this study is illustrated in Fig. 1.

2.1. Study area

SCC is the administrative centre of Sylhet Division and a major metropolitan area in the northeastern region of Bangladesh. The SCC area was chosen for this study due to its third rank among the most economically influential cities in Bangladesh after Dhaka and Chittagong (Fig. 2). It is the largest source of natural oil and gas and the most prominent hub of tea production in Bangladesh [30]. Geographically, the city is situated between 24.8976 north latitude and 91.877808 east longitude on the northern banks of the Surma River and has a subtropical climate and lush highland terrain. The study was undertaken within the city area of 26.5 km². The SCC consists of four thanas, including twenty-seven wards [30]. According to the census report of 2011, more than half a million people live in the city, and the population growth rate is 1.73% [31]. The geographical location of Sylhet is complicated, with diverse sacrificial geomorphology and Plio-Miocene aged high topography. The city is surrounded by hills and basins,

Table 2
UTFVI threshold values.

UTFVI Profile	UTFVI Value Range
None	<0
Weak	0–0.005
Middle	0.005–0.010
Strong	0.010–0.015
Stronger	0.015–0.020
Strongest	>0.020

Table 3
Comparison of different new generation prediction algorithms.

Name of the Algorithm	Correlation Equation	MSE	R
ANN	$y = 0.89*x + 0.42$	0.896	0.51
ResNet	$y = 0.89*x + 0.02$	0.890	0.53
GoogLeNet	$y = 0.87*x + 0.01$	0.862	0.61
VGGNet	$y = 0.87*x + 0.18$	0.859	0.63
AlexNet	$y = 0.85*x + 0.40$	0.850	0.69

making it one of the most distinctive areas of the country. Three distinct seasons are currently noticeable in Bangladesh, namely summer (March to June), rainy season (July to October), and winter season (November to February). Sylhet has a tropical monsoon climate, with a hot and humid rainy season (April to October). About 80% of the total rainfall in Sylhet occurs between May and September [32].

2.2. Data description

Twelve Landsat satellite imageries from 1995 to 2020 at five-year intervals were used to carry out the study. Among the imageries, eight were from Landsat 4–5 TM (during 1995–2010), and the other four were from Landsat 8 OLI Sensors (during 2015–2020). To explore the seasonal UTFVI variations during summer and winter, six images each for both summer (March–June) and winter season (December and February) (Table 1) were acquired. The images were collected from the USGS Earth Explorer website (<https://earthexplorer.usgs.gov>) to estimate the LULC and UTFVI. The cloud cover was set to less than 10% during the download process. All the data had a spatial resolution of 30 m. The detailed descriptions of the downloaded datasets are provided in Table 1.

2.3. LULC classification

The LULC classification was conducted using the SVM algorithm, which has recently gained popularity for its high classification accuracy [9]. From 1995 to 2020, the acquired images of five-year intervals were classified using the SVM algorithm. The ENVI 5.3 software was used to produce the LULC maps. SVM is a multivariate system and is reliant on training procedures [28]. In the space of the decision boundary, a peerlessly dissociable linear hyperplane is constructed at the start of the SVM process.

If k number of training samples are considered as $\{X_i, Y_i\}$, $i = 1, 2, 3, \dots, k$

A n-dimensional space is labelled as $X \in \mathbb{R}^n$.

Class label = $y \in \{-1, +1\}$

W = perpendicular to the linear hyper-plane.

Let, a scalar b be the counteraction of the hyper-plane from the origin space.

Class 1 and Class 2 be -1 and $+1$

The two formulae for the differentiation of the hyper-planes are mentioned in Equations (1) and (2)

$$WX_i + b \geq +1 \text{ for all } y = +1 \quad i.e., \text{ a number of class 1} \quad (1)$$

$$WX_i + b \leq -1 \text{ for all } y = -1 \quad i.e., \text{ a number of class 2} \quad (2)$$

As a result, certain non-linear problems remain unaffected. Kernel functions are required to overcome the constraints imposed by non-linear planes and multi-formed training samples. After converting non-linear data to linear data, mapping is performed in a different dimensional elementary space distinct from the input space. Among the kernel functions, the RBF kernel, also known as the Radial Basis Function, is chosen due to its ability to handle non-linear planes and a reduced number of computation steps [5]. Gamma's penalty parameters were set to 0.07 and 120.00, respectively, while the pyramid level was set to zero by default. The software's likelihood classification threshold was set to 0.05. The LULC types were classified into four categories such as (i) bare land (fallow land, vacant land, sand, exposed soil, and lands without any vegetation), (ii) built-up area (residential settlements, commercial settlements, industrial settlements, and other impervious surfaces) (iii) vegetation (green lands, playgrounds, grasslands, and any other green vegetation) and (iv) water body (rivers, canals, ponds, and wetlands) for 25 years. In addition, to set up further training information, the images were investigated based on their spectral and areal profiles.

2.4. UTFVI estimation

For assessing thermal characteristics of the study area, seasonal UTFVI was estimated using established equations. As UTFVI is dependent on LST output, the seasonal LST was extracted for all the Landsat images. Finally, UTFVI was estimated from the final LST output and mean value of the LST by applying Equation (3). In addition, to assess the thermal condition of the study area in a more detailed manner and identify its impacts on LULC classes, UTFVI values were categorized into six classes (i.e., none, weak, medium, strong, stronger, and strongest (Table 2) [24]).

$$\text{UTFVI} = \frac{T_s - T_m}{T_m} \quad (3)$$

where, T_s = LST and T_m = mean of the LST of the study area.

2.5. LULC prediction

The CA model was applied for the prediction of future LULC changes. The CA model is used widely by researchers worldwide due to its ability to include static and dynamic transformations of LULC [33–36]. This study performed the CA algorithm for predicting LULC changes through the Methods of Land Use Change Evaluation (MOLUSCE) plugin in QGIS software. MOLUSCE is aimed to explore, investigate and forecast LULC changes by incorporating well-known techniques such as Multi-Criteria Evaluation, Logistic Regression, CA, ANN, and Weights of Evidence techniques. MOLUSCE provides an easy-to-use user interface with specialized modules and functionality. The plugin consists of multiple processes beginning with the input module, area change analysis, modelling techniques, prediction and validation. For this research, dependent (commercial space, distance from roads/highways, slope, elevation, educational institutions, and water bodies) and independent (LULC maps) variables were used as the input module. For projecting 2025 and 2030 LULC maps, LULC maps of 2005, 2010, 2015, and 2020 were utilized. The area change investigation calculates LULC variations among two time periods, generates transition matrices and change maps. The ANN model was utilized to predict LULC transition potential changes in the modelling stage, where maximum iteration was set to 500. Neighbourhood pixel was set to 9 (3*3) cells to specify the maximum iteration and neighbourhood pixel for the model. The prediction stage provides prospective transition maps, certainty functions (experimental), and prediction results for 2025 and 2030.

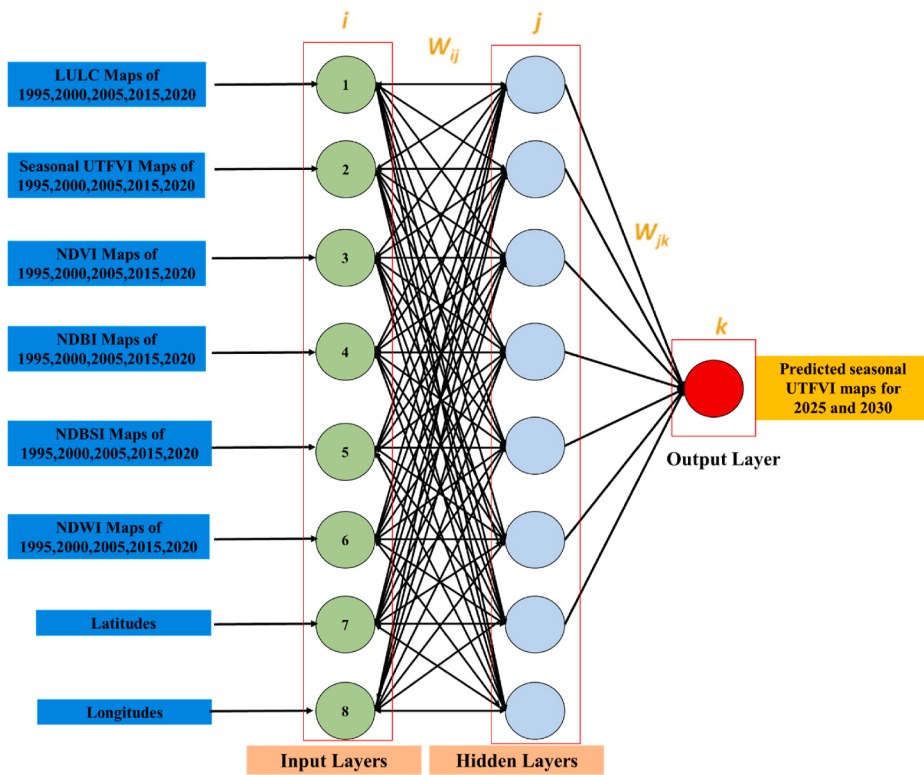


Fig. 3. Detail process of seasonal UTFVI prediction using ANN algorithm.

Table 4
Accuracy assessment of the classified LULC maps.

Year	User Accuracy (%)				Producer Accuracy (%)				Overall Classification Accuracy	Overall Kappa Coefficient (T)
	Bare Land	Built-Up Area	Vegetation	Water Body	Bare Land	Built-Up Area	Vegetation	Water Body		
1995	86.96	88.24	88.89	88.10	83.34	90.91	83.58	100	88.11%	83.8%
2000	85.11	88.89	88.46	90.91	88.89	91.80	79.31	95.24	88.35%	84.36%
2005	89.80	86.27	90.63	91.43	88	97.78	82.85	94.12	89.45%	85.68%
2010	88	90	92	92	89.80	91.83	86.80	93.87	90.50%	88.25%
2015	94	96	86	96	90.38	97.96	89.58	94.12	93%	90.67%
2020	92	89.80	86.27	95.92	90.20	93.62	89.80	90.38	90.95%	87.94%

Table 5
CA model validation using Person Chi-Square.

LULC Type	Actual map (O)	Predicted map (E)	(O-E)	(O-E) ² /E
Water Body	3.98	3.71	0.27	0.073
Built-up Area	52.66	52.04	0.62	0.384
Vegetation	40.27	41.03	-0.76	0.578
Bare Land	3.08	3.24	-0.16	0.026

$$\chi^2 = \sum(O-E)^2/E = 0.049; \text{DoF } (C-1) = 3 \text{ and } \chi^2_{0.05}(3) = 7.815.$$

Table 6
CA model validation for LULC Prediction in QGIS.

Year	Kappa parameters for model validation in Q-GIS MULUSCE Plugin			
	% Of Correctness	Kappa (histo)	Kappa (loc)	Kappa (Overall)
2015	97.1843	0.9527	0.9978	0.9507
2020	97.0784	0.9495	0.99552	0.94528

Table 7
Validation of the predicted seasonal UTFVI for the year 2020.

Prediction Year	ANN model Validation for UTFVI prediction using MATLAB software		
	No of hidden layer	RMSE	R
Summer 2020	6	0.56	0.88
Winter 2020	6	0.624	0.87

2.6. UTFVI prediction

As new generation algorithms are getting more attention for prediction related study, before applying any specific algorithm for UTFVI prediction, model performance comparison of ANN, ResNet, GoogLeNet, VGGNet, AlexNet was performed. Based on the assessment, ANN and ResNet are showing excellent output in prediction analysis. For seasonal UTFVI prediction, ANN was used in this study as the algorithm demonstrated higher accuracy than others (Table 3).

The UTFVI data sets for the years 2005, 2010, 2015, and 2020 were utilized to model the seasonal (summer and winter) UTFVI for years 2025 and 2030 using the ANN algorithm. The ANN algorithm was extensively used by researchers in prediction studies [37]. The ANN

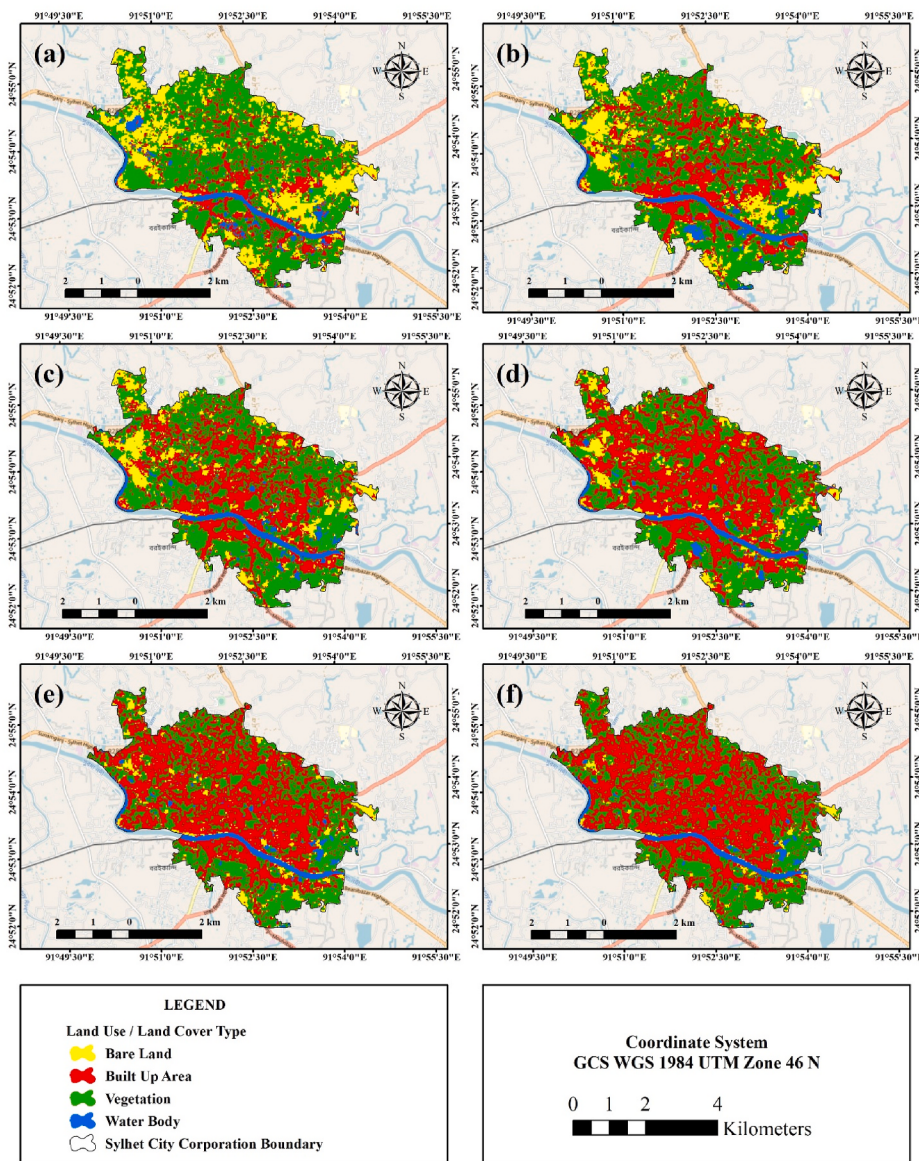


Fig. 4. LULC maps of the study area for years a) 1995 b) 2000 c) 2005 d) 2010 e) 2015 f) 2020.

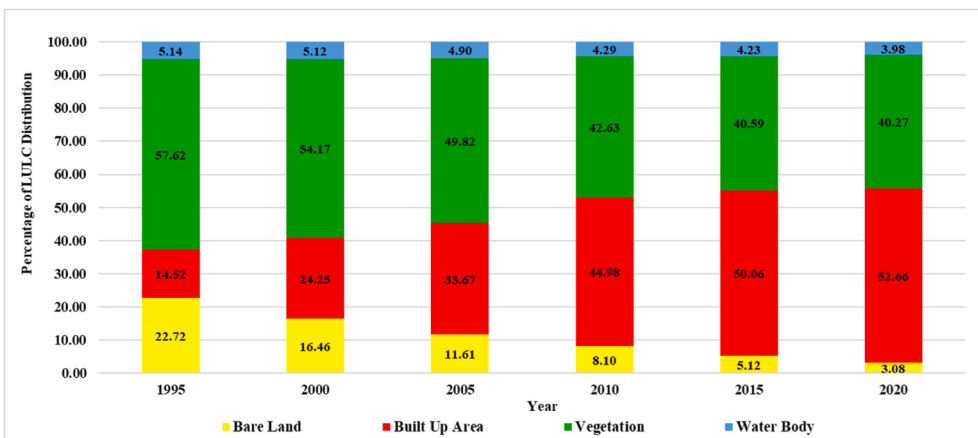


Fig. 5. Changes in LULC classes from 1995 to 2020.

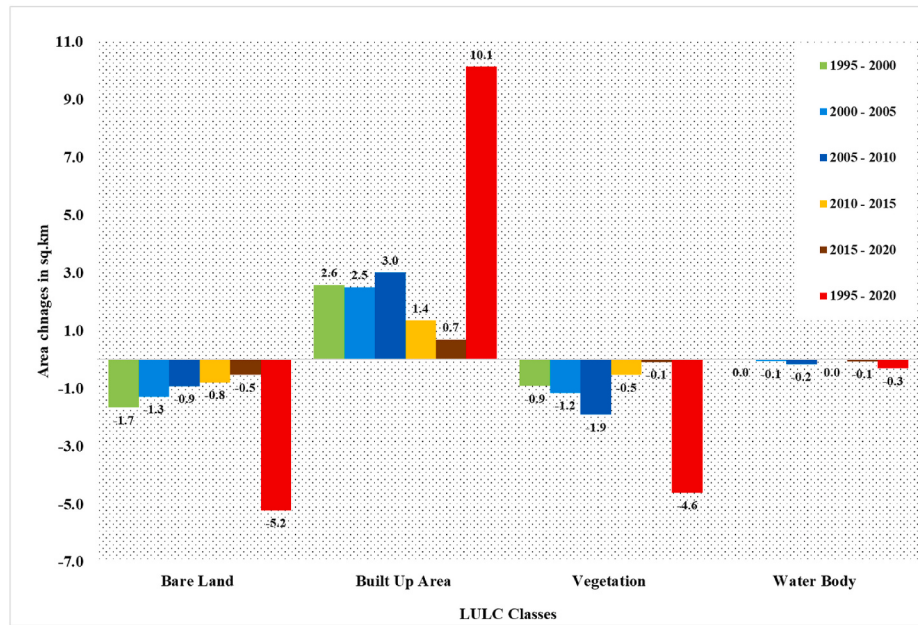


Fig. 6. Gain and loss of different LULC classes from 1995 to 2020.

comprises of Multi-Layer Perceptron (MLP) neural network technique, which makes autonomous decisions regarding network parameters and their changing patterns for better forecasting. The MLP is established on the fundamental error-correction learning principle. In MLP, the network initially provides a possibly low accuracy random output when it gets a pattern. The error function then determines the differences between this random output and the intended result. Meanwhile, the correction weights are computed between the output layer and the hidden layers and between the hidden layers and the input layers using the "Leveraging back-propagation" technique. This procedure remains until an acceptable error is achieved between the network and the intended output. The UTFVI simulation was based on the predicted seasonal temperature data patterns between 1995 and 2020. The research region was partitioned into 500 m × 500 m spatial grids in QGIS software to create the sample points. This grid size has been set to evaluate the smallest space at which one-point characteristics may affect a meaningful change in the UTFVI [38]. The sample datasets were used to create an ANN in the MATLAB program for the simulation of seasonal LST. The supporting input variables were applied for improved accuracy of the ANN model, NDBI, NDVI, NDBSI, NDWI, LULC, latitude, and longitude. The more the supporting variables, the higher will be the accuracy and efficiency of the ANN model [39]. The prediction of seasonal UTFVI using the ANN technique includes network training, network building, performance assessment, and prediction (Fig. 3). The seasonal UTFVI predicted output for the next 5 (t+5) and 10 (t+10) years, are shown mathematically in equations (3) and (4).

$$\text{UTFVI}(t+5) = f[\text{LULC}(t), \text{LULC}(t-5), \text{NDBI}(t), \text{NDBI}(t-5), \text{NDBSI}(t), \text{NDBSI}(t-5), \text{NDVI}(t), \text{NDVI}(t-5)] \dots \dots (3)$$

$$\text{UTFVI}(t+10) = f[\text{LULC}(t), \text{LULC}(t-10), \text{NDBI}(t), \text{NDBI}(t-10), \text{NDBSI}(t), \text{NDBSI}(t-10), \text{NDVI}(t), \text{NDVI}(t-10)] \dots \dots (4)$$

where t = 2020.

The algorithm's performance was evaluated using Root Mean Square Error (RMSE) and Correlation Coefficient (R). The assessment was done by comparing predicted and estimated UTFVI for 2019 mentioned. RMSE (equation (5)) and R (equation (6)) squared are the widely used metrics for measuring model performance [40].

$$RMSE = \sqrt{\frac{\sum (T_{obs} - T_{model})^2}{n}} \quad (5)$$

$$R = \left[\frac{\sum (T_{obs} - \bar{T}_{obs})(T_{model} - \bar{T}_{model})}{\sqrt{\sum (T_{obs} - \bar{T}_{obs})^2} \sqrt{\sum (T_{model} - \bar{T}_{model})^2}} \right] \quad (6)$$

2.7. Model validation

2.7.1. LULC classification validation

Kappa statistics were performed for the accuracy assessment of the classified LULC classes. The user accuracy, producer accuracy, kappa coefficient, and total accuracy were evaluated under the Kappa statistics accuracy assessment. Table 4 shows excellent results for all the years with an overall Kappa Coefficient of greater than 83%.

2.7.2. LULC prediction model validation

LULC prediction model CA accuracy performance was measured using Chi-square and Kappa parameters. Chi-square evaluates whether the predicted and reference map matched closely with each other or not. Classification accuracy evaluation was attained using Equation (7) [41–44].

$$X^2 = \sum \frac{(O - E)^2}{E} \quad (7)$$

A null hypothesis (H_0) and alternative hypothesis (H_1) was established for assessing the accuracy of the classification.

H_0 = Reference and predicted map for the year 2020 significantly match with each other

H_1 = Reference and predicted map for the year 2020 do not match with each other

Rejection level at $\alpha = 0.05$, level of significance (LoS) with a degree of freedom (DoF) 3.

The computed value of Chi-square was 0.049, which was very less than the tabulate value 7.815 of Chi-square at $\alpha = 0.05$. LoS and rejected the H_0 at 95% confidence level (Table 5). The rejection of H_0 represents that the predicted, and actual LULC map for 2020 were similar with no

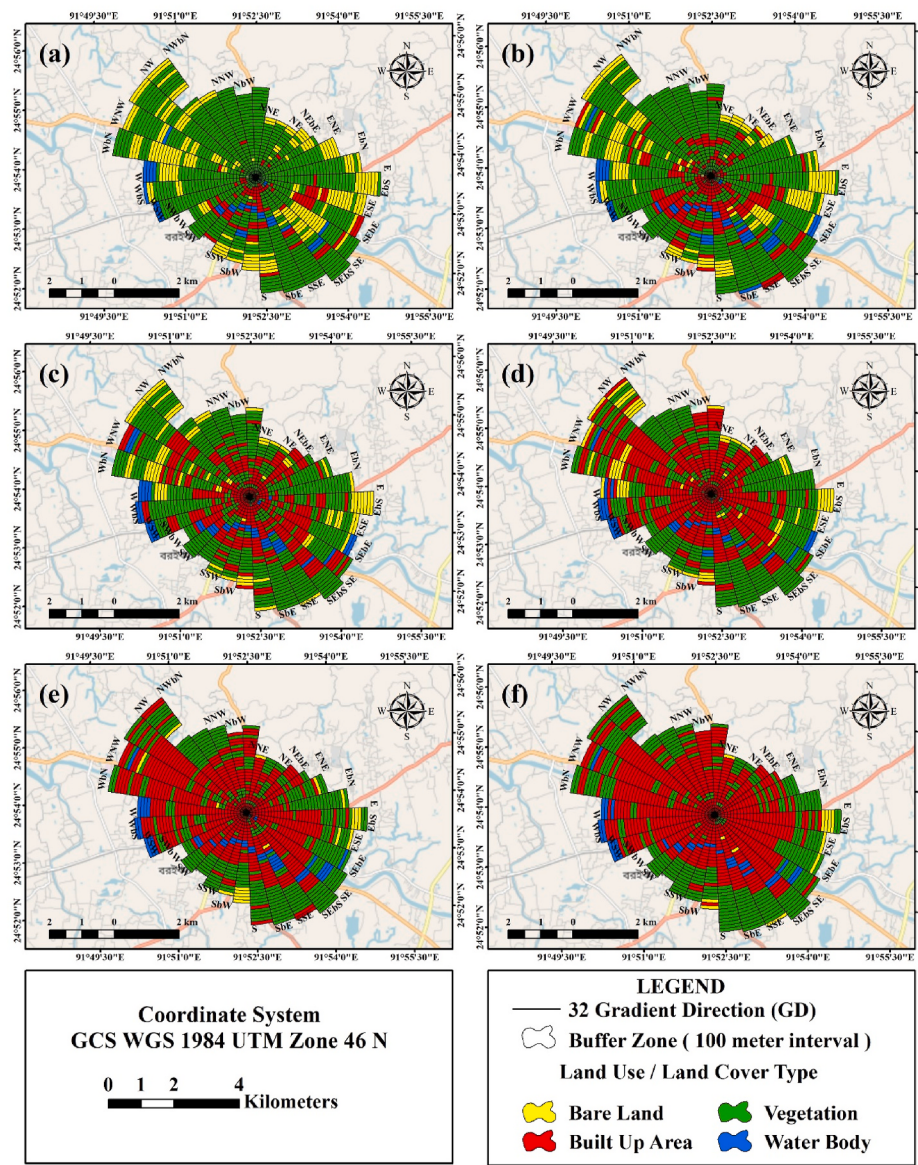


Fig. 7. Directional changes of LULC classes for years a) 1995, b) 2000, c) 2005, d) 2010, e) 2015, f) 2020.

significant difference.

CA model was also validated using kappa parameters in QGIS platform. For assessing the prediction accuracy, maps for 2015 and 2020 were predicted using (1995 & 2005) and (2000 & 2010) input datasets. Based on the prediction results by comparing the predicted with estimated datasets of 2015 and 2020, the LULC images were predicted for years 2025 and 2030 using CA algorithms. Table 6 shows the model validation of LULC prediction. According to the validation, overall Kappa statistics for 2015 and 2020 were 95.07% and 94.53%, respectively. These values were considered suitable for predicting future LULC maps with a reasonable level of accuracy.

2.7.3. UTFVI prediction model validation

The performance of the UTFVI prediction model (ANN) was conducted in MATLAB software by assessing the RMSE and R values. The predicted and actual UTFVI distribution of 2020 revealed an excellent accuracy of the model. Values of R showed excellent output with values close to 1 for the year 2020 summer and winter (Table 7). The model validation results are satisfactory to evaluate the future UTFVI expansion.

2.8. Seasonal UTFVI variations over LULC classes

The relationship between seasonal UTFVI and LULC classes were evaluated by estimating changes of UTFVI classes over different land cover. ArcGIS tabulate tool was used to establish the UTFVI variations over LULC classes. The tabulate tool applies cross-tabulation between two rasters' pixels (UTFVI and LULC) and provides output as table. The areas of the two raster datasets do not have to be contiguous.

2.9. Directional change estimation of LULC and UTFVI

A directional overview of the LULC and UTFVI changing phenomenon will help to understand the spatial distribution of respective features in a microscale fashion. The directional analysis is a helpful approach for implementing urban development projects at the micro-level for ensuring sustainability [45,46]. A ring surrounding the urban centre was drawn first with a buffer distance of 200 m interval. The ring then was divided into 16 equal parts, creating 16 individual directional inputs for spatial distribution. After intersecting the observation and data layer, a final output was revealed, showing each segment's highest percentage of respective features.

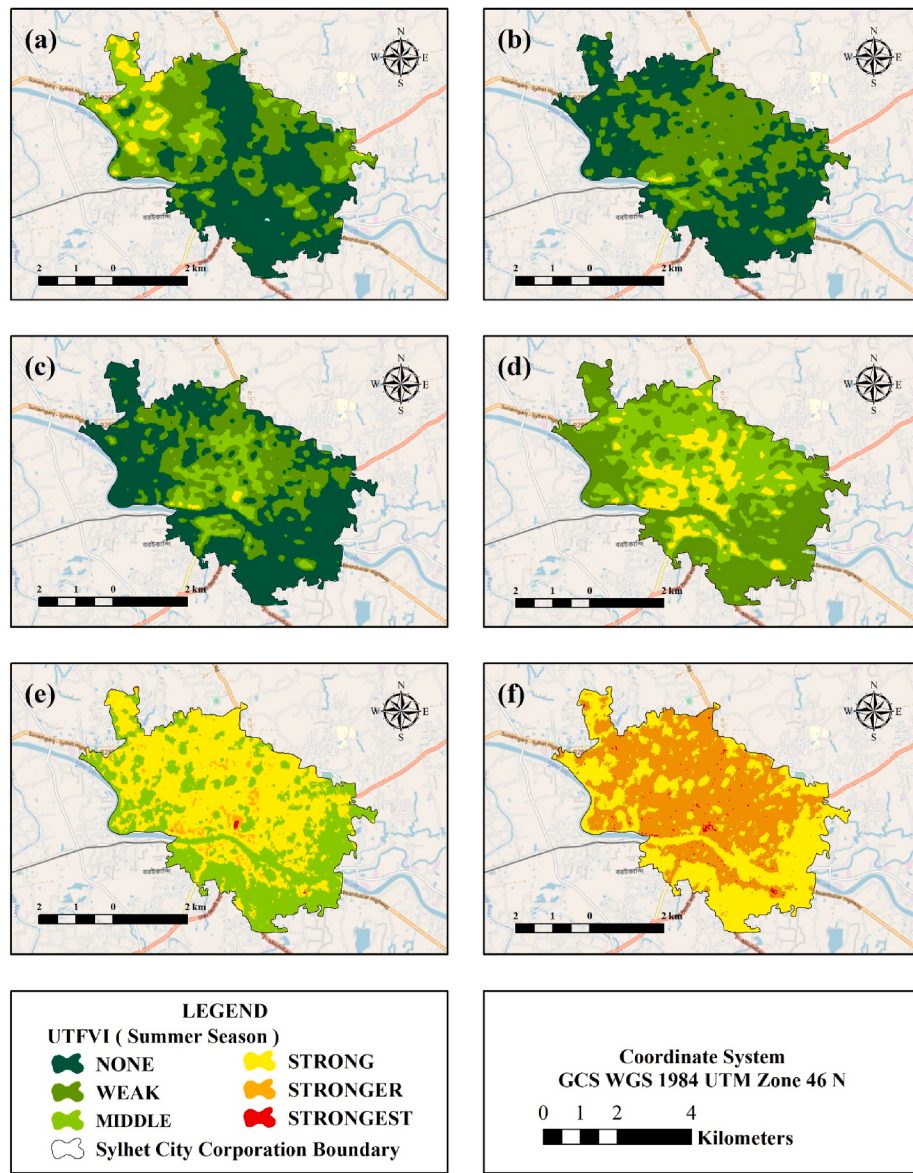


Fig. 8. Summer UTFVI variations in the study area for years a) 1995 b) 2000 c) 2005 d) 2010 e) 2015 f) 2020.

3. Result and discussion

3.1. LULC change analysis

Spatiotemporal LULC maps from 1995 to 2020 were estimated by applying SVM algorithms at 5 years intervals (Fig. 4). Two trends were noticeable from the last 25 years LULC changing pattern in the form of a dramatic increase in built-up areas and reduction of bare land, green cover and water bodies. The findings show that water bodies and vegetation areas were gradually converted to built-up areas. In 25 years, built-up areas were increased by 38.14 % and bare land, vegetation cover and water bodies were decreased by 19.64 %, 17.35 % and 1.16 % (Fig. 5).

A drastic increase in the built-up area was observed from 1995 to 2020, with the highest percentage of the increase occurring between 2005 and 2010. The built-up area expansion rate was observed more than 2.5 km^2 every five consecutive years, while the highest increase was taken place from 2005 to 2010 (3 km^2). In the last 25 years, built-up areas were significantly increased (10 km^2) by replacing bare land, green cover, and water bodies. Almost 5 km^2 of bare land and vegetation cover

were reduced from 1995 to 2020 (Fig. 6). Water bodies declined by 0.3 km^2 , which was comparatively low considering other changes. This is mainly because of the initiatives taken by SCC in the form of 114 river excavation and bank preservation under development projects.

Both strategic and economic factors influence this notable expansion of urban areas and reduction of green cover and water bodies. Factors like rural-urban migration, an increase of native urban population, the territorial extension of existing city areas, and significant upsurge in construction and development activities have been the major driving forces for such LULC transformation across the study area [47–49]. Migration and development activities are among the most influential factors contributing to the expansion of SCC urban growth. Rural people migrate to cities to get better employment opportunities and enjoy a standard quality of life. The city authority needs to ensure the planned development of urban areas by conserving existing natural resources (green cover and water bodies). In addition, urban residents must be aware of the consequences of unplanned infrastructural development by reducing natural resources and helping city authorities to ensure the environmental sustainability of Sylhet city.

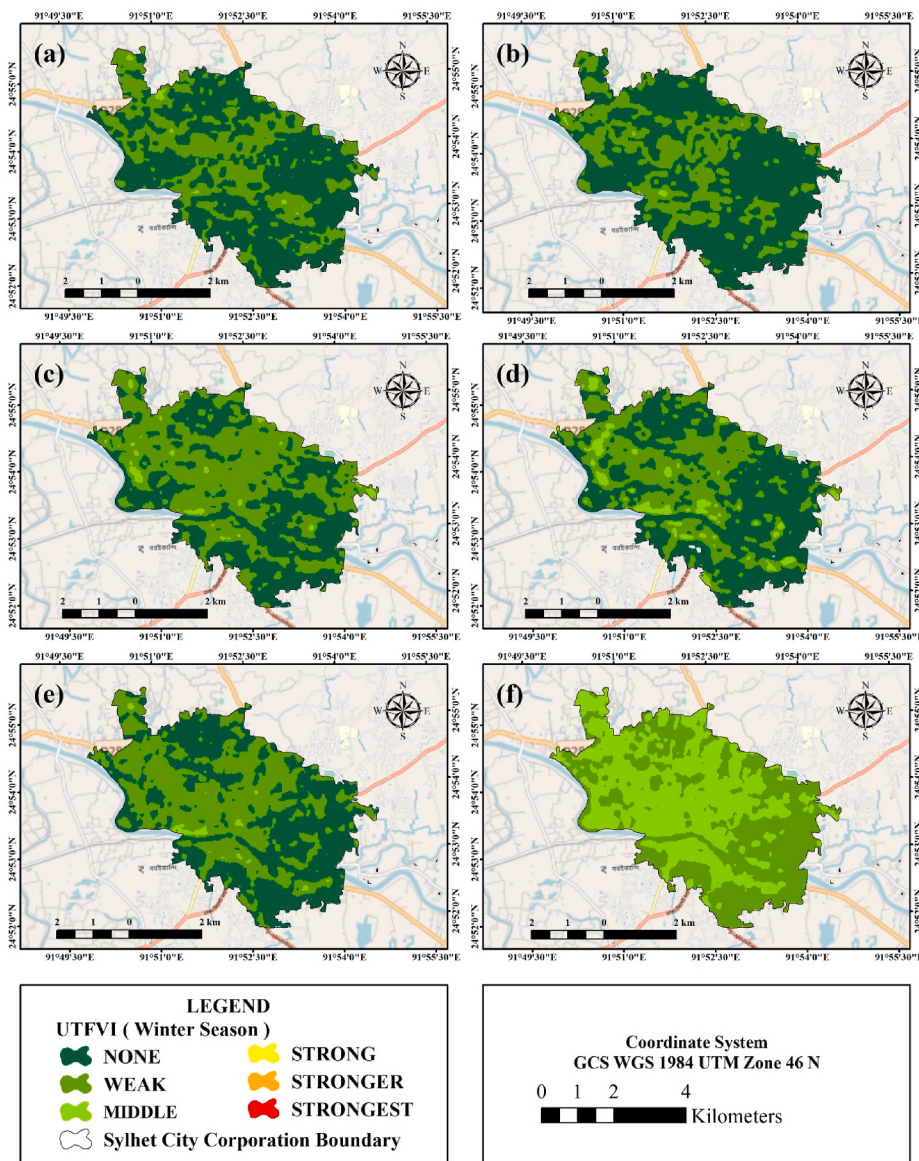


Fig. 9. Winter season UTFVI variations in the study area for years a) 1995 b) 2000 c) 2005 d) 2010 e) 2015 f) 2020.

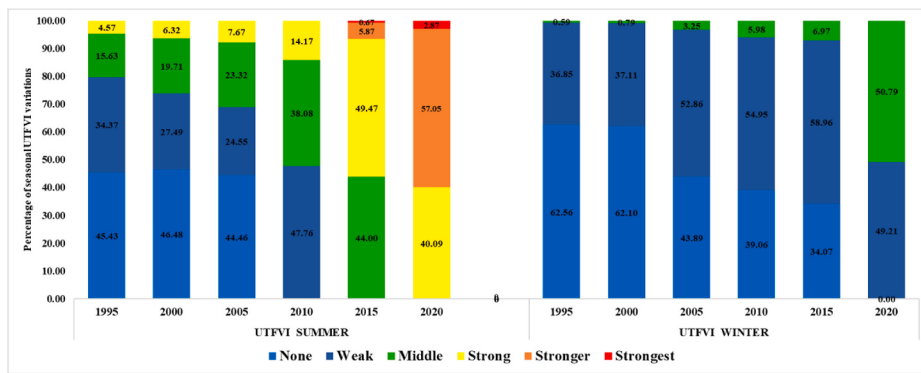


Fig. 10. Percentage of seasonal UTFVI distribution in the study area from 1995 to 2020.

3.2. Directional changes of different land cover

Assessment of directional changes is a useful approach to assess micro-scale variations of different LULC classes. This type of analysis is

mainly adopted to identify the impacts of rapid urban growth at the microscale level in growing urban areas [50,45]. To denote the change direction of LULC classes, 16 concentrated circles were drawn at each 5-km random equal interval from the city centre to the study area

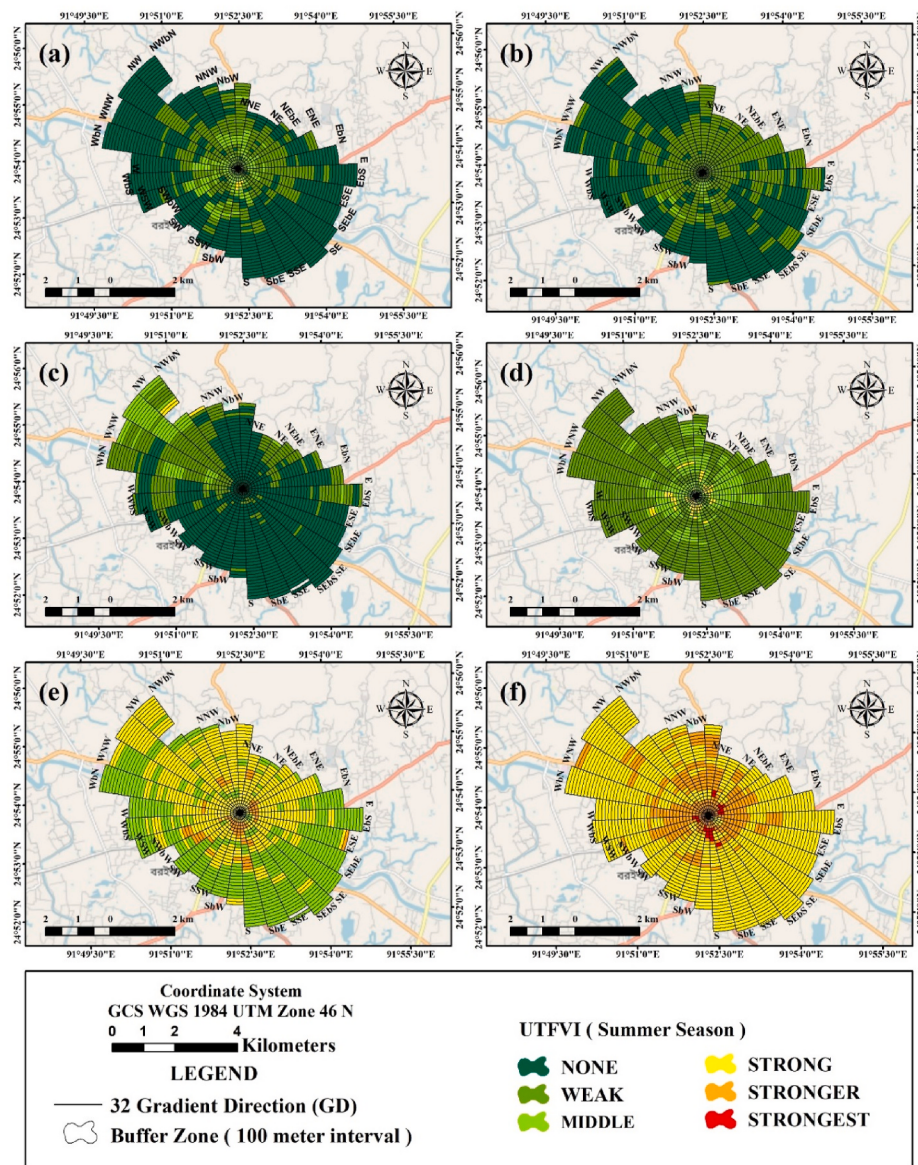


Fig. 11. Directional summer UTFVI distribution for years a) 1995 b) 2000 c) 2005 d) 2010 e) 2015 f) 2020.

boundary (Fig. 7). In 1995, the built-up area was mainly focused on the city's east, southeast, and southern parts (Fig. 7a). Between 1995 and 2000, a noticeable increase in built-up areas in all directions was identified (Fig. 7b). Between 2000 and 2005, a similar expansion was observed all around the city centre (Fig. 7c). The increase in directional changes became clear after 2010, with a high expansion of the built-up area in the northwest, west, and southwest (Fig. 7d). Although some vegetation and bare land existed in the middle and fringe areas of the city, between 2015 and 2020, most of them were replaced by built-up areas with the highest expansion in the northwest, western and southwest parts of the city. The city has less area in the northern and northeast parts, already covered with built-up areas. Although the southern and southeast part has the lowest built-up area, it is anticipated to be covered with more impervious layers in upcoming years. As per the information collected from SCC, several projects have already been undertaken in Sylhet to increase industrialization and create employment opportunities.

The projects undertaken for the development of Sylhet include but not limited to Bangabandhu Sheikh Mujib Hi-Tech Park, Dhaka-Sylhet six-lane highway, Sylhet-Tamabil four-lane highway, new BSCIC Industrial City, Road and Drain Expansion, worth Tk 1200 crore. The

development should be implemented in a planned manner by considering the sustainable replacement of green cover and water resources. Otherwise, in upcoming years, the city will face serious environmental threats.

3.3. UTFVI change estimation

The UTFVI defines the quality and degree of thermal comfort in the urban environment. Figs. 8 and 9 show the threshold values of summer and winter UTFVI distributions in SCC from 1995 to 2020 at five years intervals. The UTFVI analysis showed a significant seasonal variation in all years. In summer (1995), around 80% of the city area had no or weak UTFVI effect (Fig. 8). No significant change was observed between 1995 and 2000, but a slight rise in moderate and strong UTFVI regions was observed. The decline in none and weak UTFVI regions were continued until 2010, with approximately a 31% rise of moderate and strong UTFVI affected areas. A noticeable change was identified in 2010 as the percentage of no UTFVI affected zones became zero, and more than 50% of the areas were affected by moderate and strong UTFVI. In 2015, the weak UTFVI zones were diminished, with around 50% of strong and 6% stronger UTFVI affected zones. The thermal characteristics became

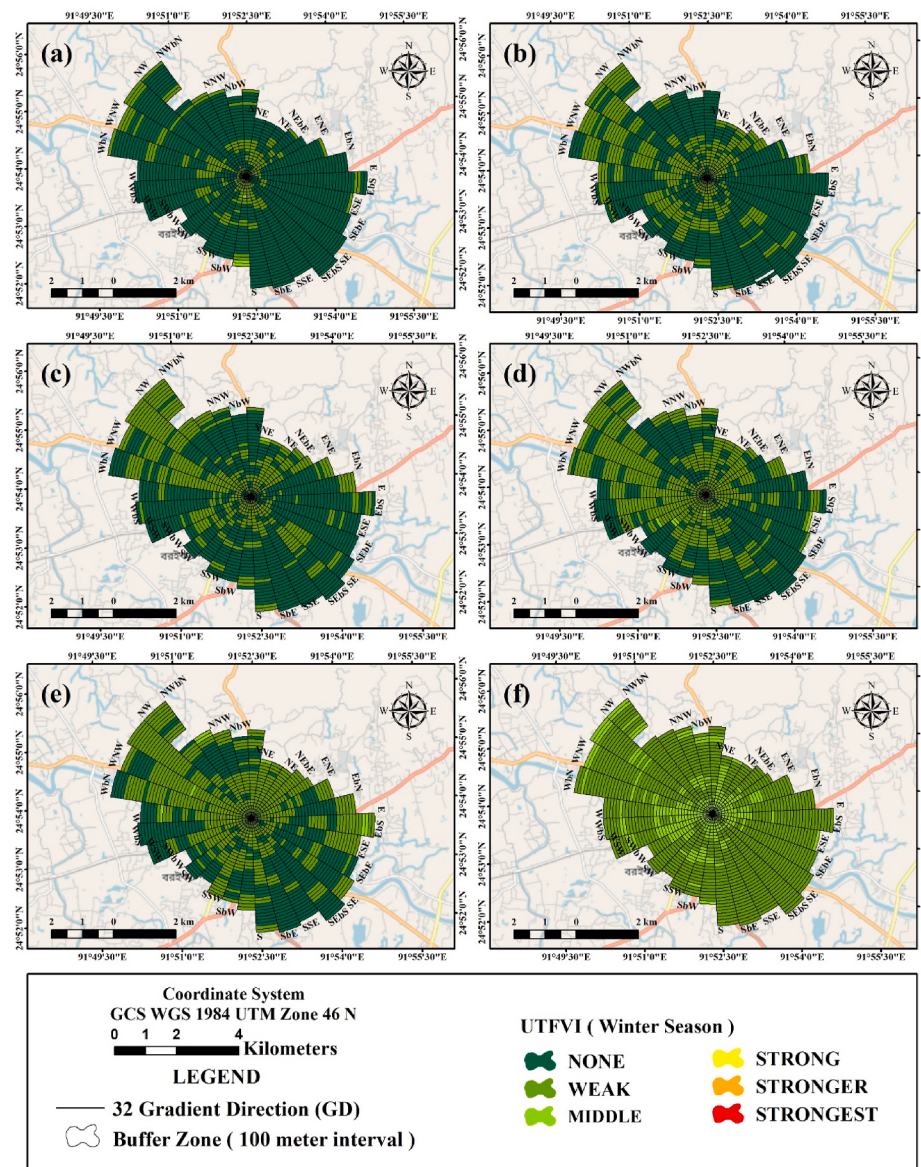


Fig. 12. Directional winter UTFVI distribution for years a) 1995 b) 2000 c) 2005 d) 2010 e) 2015 f) 2020.

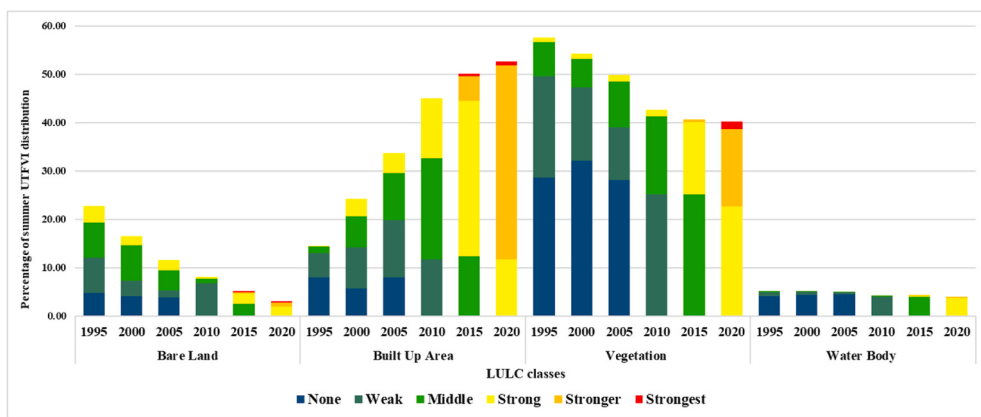


Fig. 13. Summer UTFVI distribution over LULC classes from 1995 to 2020.

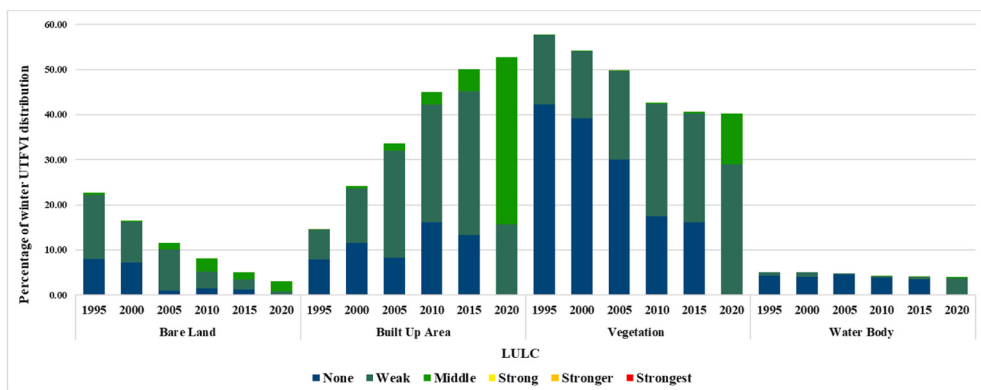


Fig. 14. Winter UTFVI distribution over LULC classes from 1995 to 2020.

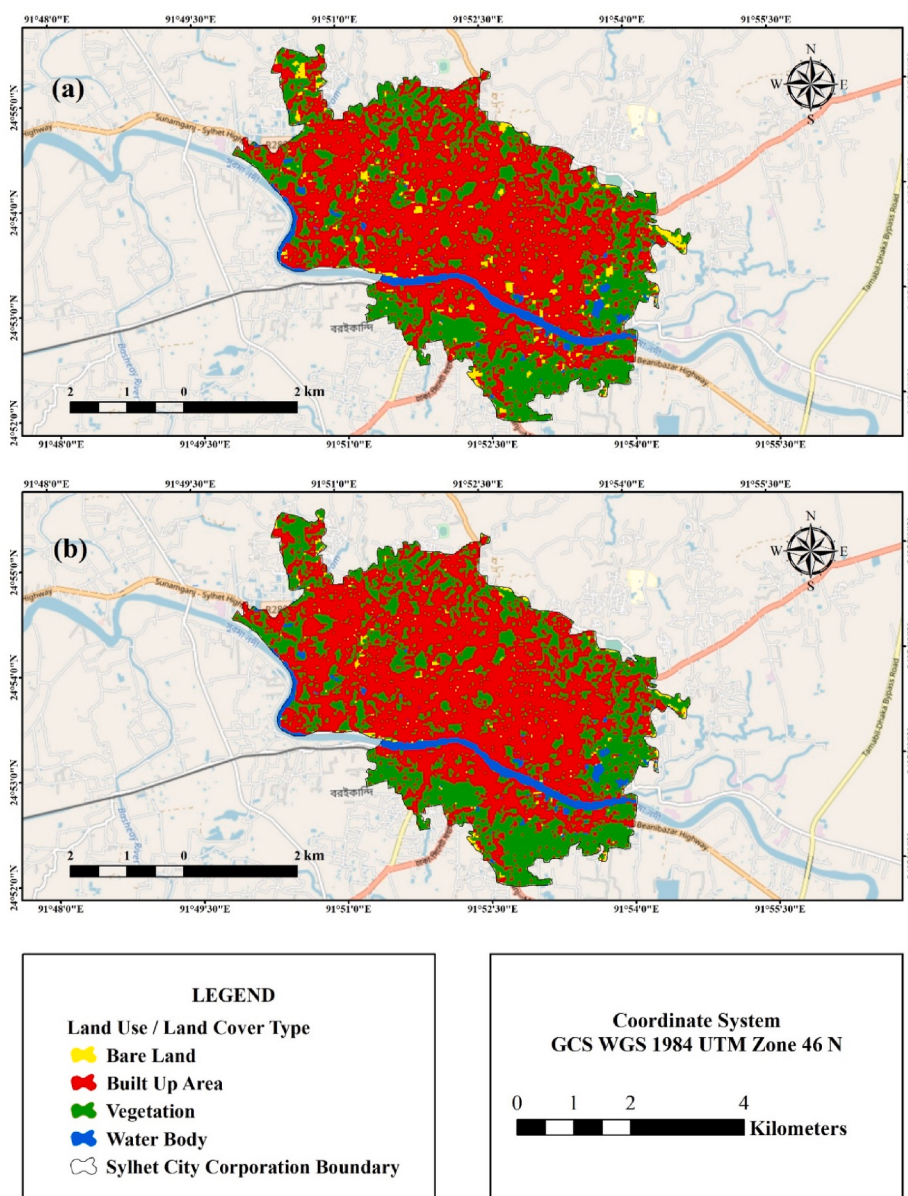


Fig. 15. Predicted LULC maps for years a) 2025 and b) 2030.

Table 8

Historical and predicted LULC statistics and change during the study period.

Year	LULC in percentage			
	Bare Land	Built Up Area	Vegetation	Water Body
1995	22.72	14.52	57.62	5.14
2000	16.46	24.25	54.17	5.12
2005	11.61	33.67	49.82	4.90
2010	8.10	44.98	42.63	4.29
2015	5.12	50.06	40.59	4.23
2020	3.08	52.66	40.27	3.98
2025	2.83	56.62	36.66	3.90
2030	1.92	58.93	35.32	3.82
Change 1995–2025	-19.89	42.09	-20.96	-1.24
Change 1995–2030	-20.79	44.41	-22.30	-1.32

worse in 2020, with an area around 57% stronger and 3% strongest, whilst the strong UTFVI regions diminished slowly.

A similar UTFVI changing pattern was observed for the winter season. In 1995, almost all the city areas were under none or weak UTFVI

zones (99.41%). A slight increase of moderate UTFVI affected areas (0.79%) was observed in 2000. The increase of moderately affected zones and the decrease of none and weak, affected zones were continued throughout 2005, 2010, and 2015. In 2020, SCC experienced a significant increase in moderate UTFVI zones with the diminish of no affected zones. Fig. 10 shows that about 50.79% of the total SCC areas were in the middle UTFVI zones, and the remaining 49.29% of the area was in the weak UTFVI zone.

Changes in thermal characteristics contribute to more extended summer and lower winter seasons, significantly impacting the study area. High temperature accelerates the use of air conditions which contributes to smog formation and leads to increased greenhouse gas (GHG) emissions. In addition, increased temperature creates health impacts in the forms of cardiovascular and respiratory disease, injuries and premature death, infectious diseases, food and waterborne illness and threat to mental health.

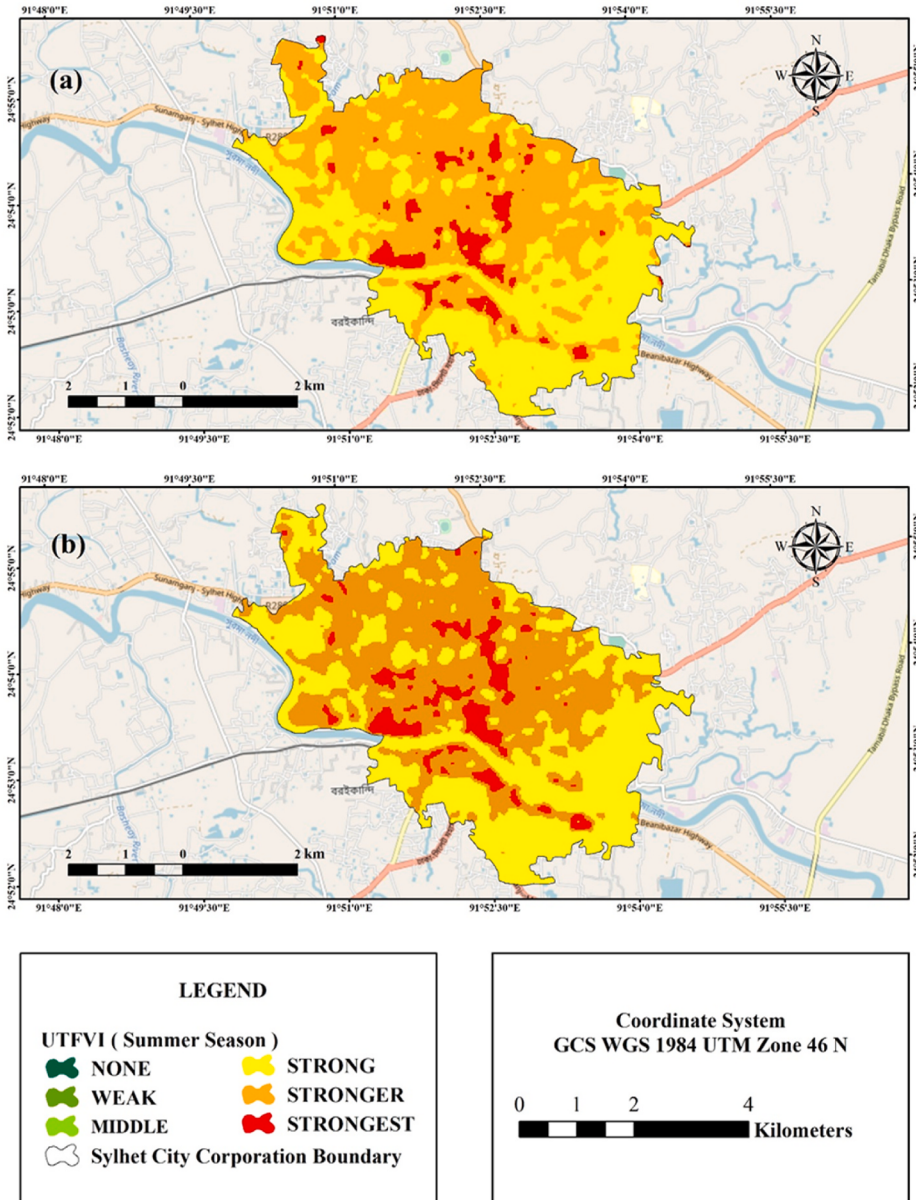


Fig. 16. Predicted summer UTFVI maps for year a) 2025 and b) 2030.

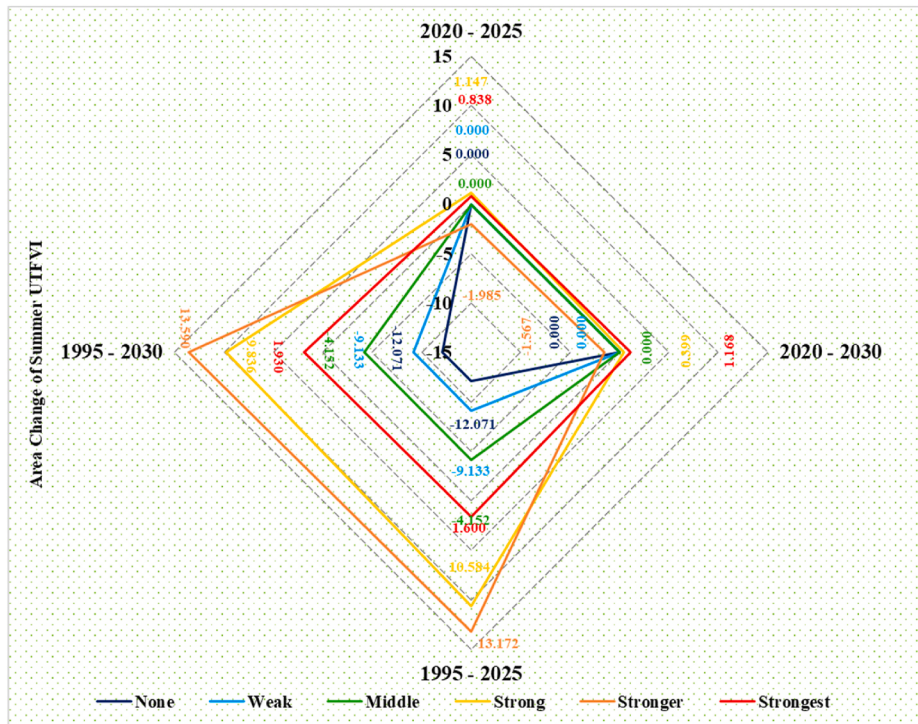


Fig. 17. Spider diagram showing the distribution of changes (km²) in summer UTFVI from 1995 to 2030.

3.4. Directional changes of UTFVI phenomenon

Directional change analysis of seasonal UTFVI is an effective approach to identify the study area's micro-scale thermal comfort variations in the last 25 years. Fig. 11 illustrates the summer season directional change of UTFVI in Sylhet from 1995 to 2020. In 1995, most of the directions had none and weak UTFVI effects, except some moderate effects in the western, southern, and southwest parts of the city. The weak UTFVI effect was started to expand in all directions, but mostly in the northern, northeast, and southern parts of the study area (Fig. 11b). In 2005, higher expansion of weak, middle, and strong UTFVI concentrations was observed in the western and northwest parts of the study area (Fig. 11c). In 2010, the weak and moderate effects were expanded in all directions of the city, with some strong UTFVI effects in the city centre (Fig. 11d). The situation became severe in 2015 as all parts of the city was covered with middle and strong UTFVI effect with strong effect expanding in the southwest, northern, and northwest parts of the city (Fig. 11e). A much stronger UTFVI scenario was observed in 2020, with a strong effect dominating across the city with the stronger and strongest effect expanding from the centre of the city.

A similar increasing pattern of directional UTFVI change was observed for the winter season (Fig. 12). In 1995, most directions had no UTFVI effect, with weak UTFVI effects in some directions (Fig. 12a). The weak UTFVI effect expansion was directed to the western, northwest, and southwest directions from the city centre in 2005 (Fig. 12b). The expansion was continued in 2005, and in 2010, some areas were started to experience a moderate UTFVI effect (Fig. 12c and d). Due to enormous urban expansion between 2010 and 2015, UTFVI effect was expanded in all directions from the growth centre. It resulted in the increase of weak UTFVI by affecting areas all over the city, with moderate effects by expanding in the southern and southwest corners of the city in between 2015 and 2020 (Fig. 12e and f). Overall, seasonal UTFVI directional analysis shows a continuous decrease in thermal comfort of the study area from the city centre to the outer parts of the city.

In addition to human activities, climate change contributes to temperature increases [10]. Global climate change accelerated the glacier shrunk, and trees are flowering sooner, ice on lakes and rivers is

breaking up earlier, animal and plant ranges have shifted. Climate change also amplified extreme heat stress and urban flooding due to heavy precipitation and sea level rises in coastal cities [23].

3.5. UTFVI distribution over different land cover classes

This study also documented the distributions of UTFVI classes under different LULC categories for both the summer and winter seasons. Fig. 13 shows the summer UTFVI distribution over LULC classes from 1995 to 2020. For each LULC class, the none, weak and moderate UTFVI effects were gradually diminished and turned into strong, stronger, and strongest effects. The distribution analysis shows that the effects of UTFVI was increased mainly in the built-up areas. In 1995, the built-up area had 7.92% none and 5.11% weak UTFVI areas with an average percentage of moderate effects. None affected areas were decreased in 2000, and the weak effect was increased to 8.54%, moderate UTFVI affected areas to 6.38%, and strong affected areas to 3.56%. The overall percentage was increased in all the UTFVI categories in 2005, specifically the moderate (11.83%) and strong (9.73%) affected areas. None UTFVI affected area was diminished in 2010 with an excessive increase in moderate (21.02%) and strong (12.28%) effect. The weak UTFVI affected area was also diminished in 2015, with 32.2% of the built-up area possessing a strong UTFVI effect, including some stronger and strongest affected regions. In 2020, the strong, stronger, and strongest affected area percentages were 11.75%, 40.01%, and 0.9%, respectively. Similar UTFVI distribution changing pattern was observed for vegetation. In 25 years, the none and weak affected areas were diminished by 28.68% and 20.95%, respectively. In 2020, the strong, stronger, and strongest areas dominated with 22.62%, 15.96%, and 1.69% of SCC areas, respectively. The water bodies and bare land were also experienced a continuous rise in UTFVI.

The results for winter can be explained from Fig. 14. The UTFVI effect was limited to none, weak and moderate for winter in all the assessed years. The moderate UTFVI effect was increased following the summer, and none UTFVI was decreased over the years. The none affected bare land was diminished in 2020, where in 1995, it was the highest percentage (8.01%). Similar pattern was observed from the

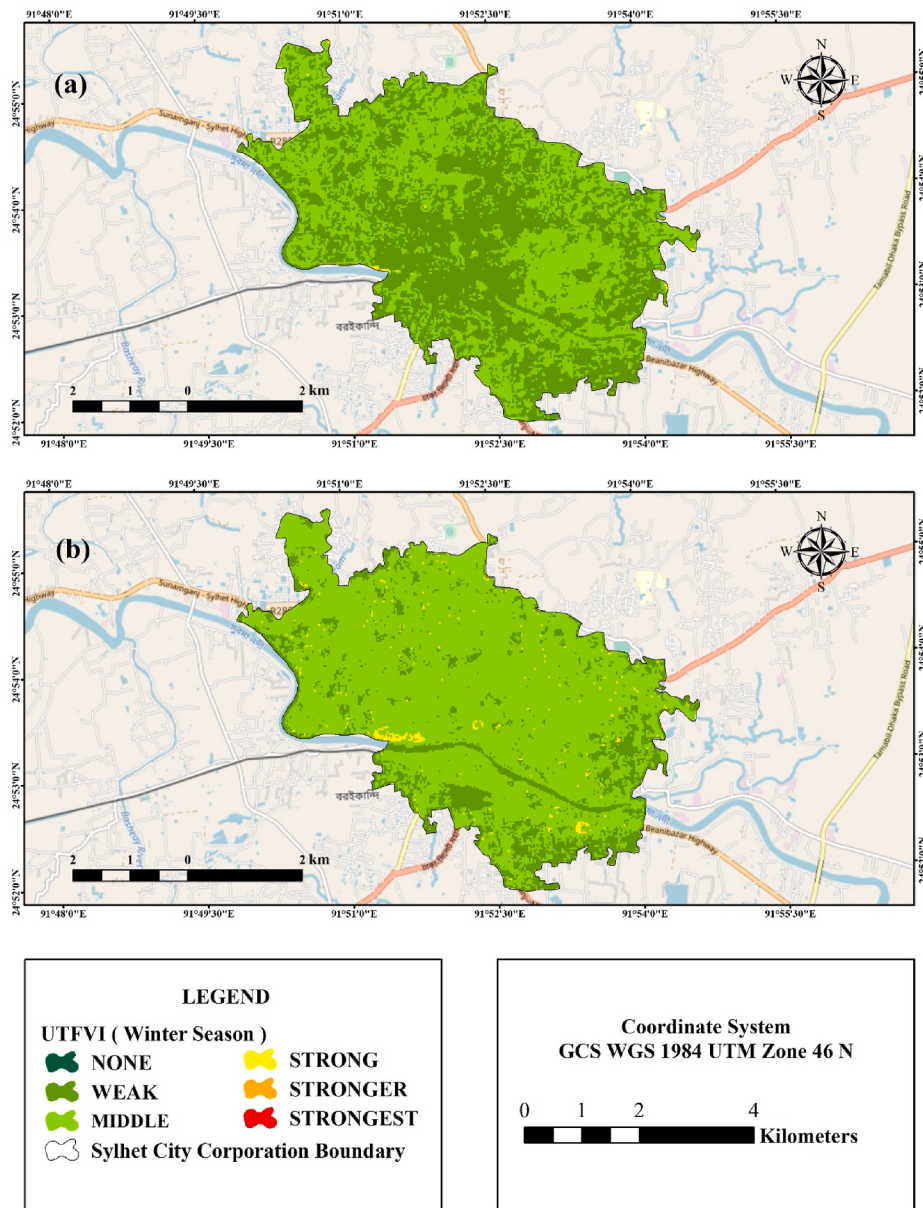


Fig. 18. Predicted winter UTFVI maps for year a) 2025 and b) 2030.

other land cover classes. During the study years, the least change was observed in weak UTFVI affected areas for all the LULC classes. Moderate UTFVI effect was increased from 0.06% to 36.98% for built-up areas and 15.29%–28.92% for vegetation. Overall analysis shows that the effects of UTFVI substantially increased due to the increase of built-up areas.

Human activities significantly contribute to the increase of cities' temperature. Cities face more UHI effects than rural areas due to more buildings and pavements. The UHI effects are mainly caused by the materials used in infrastructure development absorbing more heat than green areas and water bodies. Due to the extensive infrastructure development, GHGs are trapping the urban environment and leading to higher temperatures worldwide. Strategies need to be taken in the form of using more renewable sources instead of fossil fuels, reducing GHG emissions by increasing green spaces, incorporating sustainable water sensitive design practices into urban planning and using reflective building materials in new developments will play an influential role in reducing the UHI effects influenced by rapid infrastructural development in the study area and worldwide cities.

3.6. Prediction scenario of future LULC

The CA-ANN method was used to predict LULC conversion in the research regions in 2025 and 2030. Fig. 15 illustrates the LULC prediction map for the years 2025 and 2030. The built-up area was expected to expand towards the peri-urban areas for urbanization and socio-economic development. Compared to previous years, the built-up areas will significantly increase, and other LULC types will undergo transformation into built-up covers. Table 8 shows that the built-up area will be increased to 56.62% of the SCC area, and by 2030. Other LULC classes will experience a decrease in vegetation, decreasing from 40.27% to 36.66% by 2025 and 35.32% by 2030. In 30 and 35 years, the total built-up area will increase around 42.09% and 44.41%, respectively, with a loss of 22.30% vegetation, 20.79% of bare land, and 1.32% of water body areas. Overall prediction indicates the continuation of built-up area expansion and declination of other LULC classes.

The LULC prediction results indicate a continuation of built-up area expansion and reduction of other land cover classes. Due to the increase of more human-induced infrastructure development, the temperature

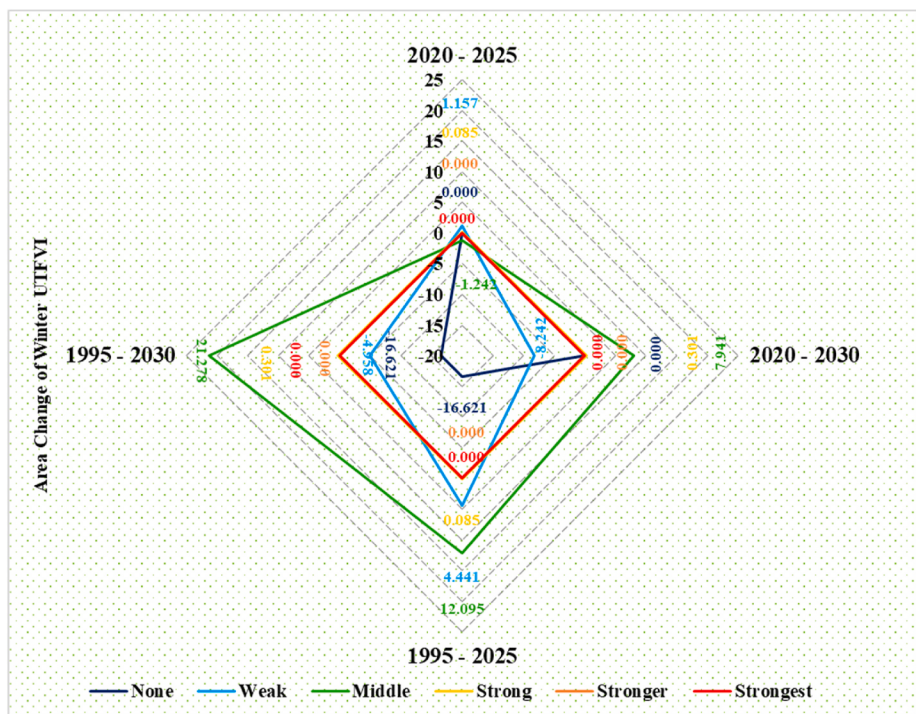


Fig. 19. Spider diagram showing the distribution of changes (km^2) in winter UTFVI from 1995 to 2030.

will continue to upsurge and accelerate the sea level rise. Sea-level rise could wash away beaches and affect recreational activities, and job losses depend on beaches in the coastal/sea adjacent region. In addition, increased infrastructural development in association with climate change will change the precipitation patterns, intensify the water cycle, bring more rainfall and associated flooding as well as drought. Proper adaptation and mitigation strategies through inclusive city master plan and climate resilience action plan need to be adopted to ensure sustainable and livable urban environment in future.

3.7. Prediction scenario of future UTFVI change

The seasonal and historical UTFVI change analysis indicates the drastic change of the thermal environment of the study area during 1995–2020. Therefore, it is essential to predict future potential UTFVI distributions across the study area. The UTFVI prediction for 2025 and 2030 was conducted using the ANN method in MATLAB. Several factors influence the thermal environment of an urban area. According to previous literature, the rapid and unplanned changes in the urban landscape have substantial impacts on increasing surface temperature [9,23, 51]. Fig. 16 illustrates that the predicted summer UTFVI maps for 2025 and 2030 will likely show that the none, weak, and middle UTFVI zones will be squeezed in the predicted years. Compared to 2020 (Fig. 8f), greater domination of the high UTFVI effect can be observed in summer 2025 and 2035. The spider diagram (Fig. 17) shows that the stronger UTFVI affected area will be decreased between 2020 and 2025. Between 2020 and 2030, the strongest UTFVI affected area will likely to be increased by 0.838 km^2 and 1.168 km^2 . In the 35-year (1995–2030), the weak and middle UTFVI affected areas will be decreased by 18.266 km^2 and 8.304 km^2 , respectively. On the other hand, the strong, stronger, and strongest affected areas will be increased by around 20.42 km^2 , 26.762 km^2 , and 3.53 km^2 , respectively. This demonstrates that if the rapid urbanization in the SCC area is not curbed rationally, it will undoubtedly aggravate the UTFVI effects.

The predicted winter UTFVI distribution for 2025 and 2030 (Fig. 18) also indicates the substantial declination in thermal comfort zones of the study area. Similar to the summer season, the study area will face the

rise of high UTFVI effects across the city in the future. Although the winter season UTFVI prediction shows no possibility of stronger and strongest UTFVI effects, the middle and strong UTFVI affected areas will significantly rise in 2025 and 2030. Between 1995 and 2025, the middle and strong UTFVI affected zones will increase by around 12.095 km^2 and 0.085 km^2 , followed by 21.278 km^2 and 0.301 km^2 between 1995 and 2030 (Fig. 19).

Overall prediction results indicate a gradual increment of higher UTFVI affected areas for both summer and winter. Warmer temperatures are an ominous sign for the urban environment and public health. Increased temperature damages ecological stability, decreases rainfall, reduces agricultural yields, declines water availability which has economic and environmental impacts and increases the probability of urban flooding and drought impacts. Warmer temperatures accelerate heat cramps, heat stroke or even death. In a nutshell, extreme heat will affect the urban environment, health, food supplies, energy demand, utility facilities and economy. By using the analysis and findings provided in this paper, city authorities can easily identify the most vulnerable areas influenced by higher temperatures and take appropriate measures to minimize the impacts of extreme heat.

4. Conclusion

Assessment and prediction related studies of spatio-temporal seasonal UTFVI variations over major Bangladesh cities are absent. As cities in Bangladesh are the key to economic advancement and face rapid population growth mostly in a haphazard manner, they are more vulnerable to unplanned LULC changes, which leads to adverse environmental impacts. Changes in cities' natural resources (green cover and water bodies) significantly impact temperature increase, which directly and indirectly affects the residents.

This research studied the LULC changes and explored the link with seasonal UTFVI in Sylhet from 1995 to 2020. The cross-linkage study was undertaken to determine the connection between LULC categories and UTFVI. By analyzing 25 years of data, the study identified that the city's green cover and water resources play a significant role in reducing UTFVI impacts where increment in urban built-up areas contributes

largely to a higher temperature. The CA model was applied to predict the future distribution of LULC in Sylhet city for 2025 and 2030, which indicated a considerable drop in green cover and a rapid increase in urban areas. The ANN model was used to estimate the future seasonal UTFVI distribution, revealing that more than 40% of the city area would likely be face higher temperatures (summer) in the form of strongest UTFVI.

To make the study results a helping tool for the urban planners in developing sustainable strategies for cities in Bangladesh, several recommendations can be followed to minimize UTFVI effects. Providing appropriate landscapes by increasing the green coverage is one of the most effective strategies to mitigate the urban microclimate effects. Proper plantation, rooftop gardening and shading from trees can expressively decrease the energy prerequisite for cooling, decrease the rate of heat convection inside buildings because of shaded surfaces and decrease the radiation exchange of the wall with the sky. An increased number of water bodies may also assist in reducing the temperature due to their evaporative action and enhanced wind speed. Again, as the heat absorption capacity of water is high, it will help to reduce the urban temperature significantly. Using high albedo roofing/pavements (white coloured roofs) materials as dark roofs absorb more heat from the sunlight and light coloured roofs do not get warmed significantly by reflecting solar radiation. The findings will allow the local government to establish an eco-friendly, sustainable environment through functional modification and replacement of the LULC distribution depending on the present circumstances. The optimal distribution of LULC directly aids in minimizing the UHI effects, sustainable city growth, conservation of ecological services, and overall citizen wellbeing. This study will provide valuable insights for government officials, city planners, policymakers, and environmental engineers.

CRediT authorship contribution statement

Abdulla - Al Kafy: Writing – review & editing, Writing – original draft, Validation, Supervision, Methodology, Investigation, Formal analysis, Data curation, Conceptualization. **Milan Saha:** Visualization, Validation, Software, Resources, Methodology, Formal analysis, Data curation. **Abdullah-Al- Faisal:** Writing – review & editing, Writing – original draft, Validation, Supervision, Resources, Project administration. **Zullyadini A. Rahaman:** Visualization, Validation, Supervision, Resources, Project administration, Funding acquisition, Conceptualization. **Muhammad Tauhidur Rahman:** Writing – review & editing, Writing – original draft, Validation, Supervision, Investigation, Conceptualization. **Desheng Liu:** Writing – review & editing, Validation, Supervision, Methodology, Investigation. **Md. Abdul Fattah:** Writing – review & editing, Writing – original draft, Validation, Resources, Methodology. **Abdullah Al Rakib:** Writing – review & editing, Writing – original draft, Visualization, Resources. **Ahmad E. AlDousari:** Funding acquisition, Project administration, Writing – review & editing. **Sk Nafiz Rahaman:** Writing – original draft, Validation. **Md Zakaria Hasan:** Writing – original draft. **Md Ahsanul Karim Ahsan:** Writing – original draft, Validation, Project administration, Data curation.

Declaration of competing interest

The authors declare that they have no known competing financial interests or personal relationships that could have appeared to influence the work reported in this paper.

Acknowledgement

The authors would like to thank the Sylhet City Corporation, Bangladesh Meteorological Department, and the US Geological Survey for assisting this research with datasets. The authors would also like to thank Dynamic Institute of Geospatial Observation Network – DIGON (<http://digonresearch.org/>) research and consultancy firm experts for

proofreading the manuscript and providing technical support in this research.

References

- [1] R. Rasool, A. Fayaz, M. ul Shafiq, H. Singh, P. Ahmed, Land use land cover change in Kashmir Himalaya: linking remote sensing with an indicator based DPSIR approach, *Ecol. Indicat.* 125 (August 2020) (2021), 107447, <https://doi.org/10.1016/j.ecolind.2021.107447>.
- [2] A-A Kafy, et al., Impact of vegetation cover loss on surface temperature and carbon emission in a fastest-growing city, Cumilla, Bangladesh, *Build. Environ.* 208 (2021) 108573, <https://doi.org/10.1016/j.buildenv.2021.108573>. In this issue.
- [3] B. Halder, J. Bandyopadhyay, Evaluating the impact of climate change on urban environment using geospatial technologies in the planning area of Bilaspur, India, *Environ. Challenges* 5 (September) (2021), 100286, <https://doi.org/10.1016/j.envc.2021.100286>.
- [4] J. Tang, L. Di, M.S. Rahman, Z. Yu, Spatial-temporal landscape pattern change under rapid urbanization, *J. Appl. Remote Sens.* 13 (2) (2019) 1, <https://doi.org/10.1117/1.jrs.13.024503>.
- [5] S. Shastry, P. Singh, P. Verma, P. Kumar Rai, A.P. Singh, Land cover change dynamics and their impacts on thermal environment of Dadri block, Gautam budh Nagar, India, *J. Landsc. Ecol. Republic* 13 (2) (2020) 1–13, <https://doi.org/10.2478/jlecol-2020-0007>.
- [6] MS Rahman, Classification of cities in Bangladesh based on remote sensing derived spatial characteristics, *J. Urban Manag.* 8 (2) (2019) 206–224, <https://doi.org/10.1016/j.jum.2018.12.001>.
- [7] N. Mundhe, R.G. Jaybhaye, N.N. Mundhe, Impact of urbanization on land use/land covers change using Geo-spatial techniques, *Int. J. Geomatics Geosci.* 5 (1) (2014) 50–60 [Online]. Available: <https://www.researchgate.net/publication/281320790>.
- [8] A-A Kafy, et al., Monitoring the effects of vegetation cover losses on land surface temperature dynamics using geospatial approach in Rajshahi City, Bangladesh, *Environ. Challenges* 4 (March) (2021), 100187, <https://doi.org/10.1016/j.envc.2021.100187>.
- [9] A.-A. Faisal, et al., Assessing and predicting land use/land cover, land surface temperature and urban thermal field variance index using Landsat imagery for Dhaka Metropolitan area, *Environ. Challenges* 4 (April) (2021), 100192, <https://doi.org/10.1016/j.envc.2021.100192>.
- [10] A-A Kafy, et al., Prediction of seasonal urban thermal field variance index using machine learning algorithms in Cumilla, Bangladesh, *Sustain. Cities Soc.* 64 (September 2020) (2021), <https://doi.org/10.1016/j.scs.2020.102542>.
- [11] C.M. Viana, S. Oliveira, S.C. Oliveira, J. Rocha, Land use/land cover change detection and urban sprawl analysis, *Spat. Model. GIS R Earth Environ. Sci.* (2019) 621–651, <https://doi.org/10.1016/b978-0-12-815226-3.00029-6>.
- [12] S. Wittke, X. Yu, M. Karjalainen, J. Hyppä, E. Puttonen, Comparison of two-dimensional multitemporal Sentinel-2 data with three-dimensional remote sensing data sources for forest inventory parameter estimation over a boreal forest, *Int. J. Appl. Earth Obs. Geoinf.* 76 (2019) 167–178, <https://doi.org/10.1016/j.jag.2018.11.009>.
- [13] D.M.S.L.B. Dissanayake, T. Morimoto, M. Ranagalage, Y. Murayama, Land-use/land-cover changes and their impact on surface urban heat islands: case study of Kandy City, Sri Lanka, *Climate* 7 (8) (2019) 1–20, <https://doi.org/10.3390/clit080099>.
- [14] S. Guha, H. Govil, A. Dey, N. Gill, Analytical study of land surface temperature with NDVI and NDBI using Landsat 8 OLI and TIRS data in Florence and Naples city, Italy, *Eur. J. Remote Sens.* 51 (1) (2018) 667–678, <https://doi.org/10.1080/22797254.2018.1474494>.
- [15] F. Najafzadeh, A. Mohammadzadeh, A. Ghorbanian, S. Jamali, Spatial and temporal analysis of surface urban heat island and thermal comfort using landsat satellite images between 1989 and 2019: a case study in tehran, *Rem. Sens.* 13 (2021) 21, <https://doi.org/10.3390/rs13214469>.
- [16] A. Dewan, G. Kiselev, D. Botje, Diurnal and seasonal trends and associated determinants of surface urban heat islands in large Bangladesh cities, *Appl. Geogr.* 135 (2021), 102533, <https://doi.org/10.1016/j.apgeog.2021.102533>.
- [17] F. Estrada, W.J.W. Botzen, R.S.J. Tol, A global economic assessment of city policies to reduce climate change impacts, *Nat. Clim. Change* 7 (6) (2017) 403–406, <https://doi.org/10.1038/nclimate3301>.
- [18] A. Pyrgou, P. Hadjinicolaou, M. Santamouris, Urban-rural moisture contrast: regulator of the urban heat island and heatwaves' synergy over a mediterranean city, *Environ. Res.* 182 (2020), <https://doi.org/10.1016/j.envres.2019.109102>.
- [19] Y. Yang, et al., Modulations of surface thermal environment and agricultural activity on intraseasonal variations of summer diurnal temperature range in the Yangtze River Delta of China, *Sci. Total Environ.* 736 (2020), <https://doi.org/10.1016/j.scitotenv.2020.139445>.
- [20] P. Kabano, S. Lindley, A. Harris, Evidence of urban heat island impacts on the vegetation growing season length in a tropical city, *Landsc. Urban Plann.* 206 (2021), <https://doi.org/10.1016/j.landurbplan.2020.103989>.
- [21] A. Dewan, G. Kiselev, D. Botje, G.I. Mahmud, M.H. Bhuiyan, Q.K. Hassan, Surface urban heat island intensity in five major cities of Bangladesh: patterns, drivers and trends, *Sustain. Cities Soc.* 71 (April) (2021), 102926, <https://doi.org/10.1016/j.scs.2021.102926>.
- [22] E.S. Im, J.S. Pal, E.A.B. Eltahir, Deadly heat waves projected in the densely populated agricultural regions of South Asia, *Sci. Adv.* 3 (8) (2017), <https://doi.org/10.1126/sciadv.1603322>.

- [23] M.N.H. Naim, A.-A. Kafy, Assessment of urban thermal field variance index and defining the relationship between land cover and surface temperature in Chattogram city: a remote sensing and statistical approach, Environ. Challenges 4 (April) (2021), 100107, <https://doi.org/10.1016/j.envc.2021.100107>.
- [24] L. Liu, Y. Zhang, Urban heat island analysis using the landsat TM data and ASTER Data: a case study in Hong Kong, Rem. Sens. 3 (2011), <https://doi.org/10.3390/rs3071535>.
- [25] H. Liu, Q. Weng, Enhancing temporal resolution of satellite imagery for public health studies: a case study of West Nile Virus outbreak in Los Angeles in 2007, Remote Sens. Environ. 117 (2012) 57–71, <https://doi.org/10.1016/j.rse.2011.06.023>.
- [26] S. Talukdar, et al., Land-use land-cover classification by machine learning classifiers for satellite observations-A review, Rem. Sens. 12 (7) (2020) 1135, <https://doi.org/10.3390/rs12071135>.
- [27] L. Ma, M. Li, X. Ma, L. Cheng, P. Du, Y. Liu, A review of supervised object-based land-cover image classification, ISPRS J. Photogrammetry Remote Sens. 130 (2017) 277–293, <https://doi.org/10.1016/j.isprsjprs.2017.06.001>.
- [28] G. Mountrakis, J. Im, C. Ogole, Support vector machines in remote sensing: a review, ISPRS J. Photogrammetry Remote Sens. 66 (3) (2011) 247–259, <https://doi.org/10.1016/j.isprsjprs.2010.11.001>.
- [29] A.W. Sejati, I. Buciori, I. Rudiarto, The spatio-temporal trends of urban growth and surface urban heat islands over two decades in the Semarang Metropolitan Region, Sustain. Cities Soc. 46 (2019), <https://doi.org/10.1016/j.scs.2019.101432>.
- [30] Sylhet | Bangladesh | Britannica. <https://www.britannica.com/place/Sylhet>. (Accessed 18 October 2021).
- [31] BBS, Bangladesh Population and Housing Census 2011, vol. 3, Urban Area Report, 2011.
- [32] S. Gupta, S. Islam, M.M. Hasan, Analysis of impervious land-cover expansion using remote sensing and GIS: a case study of Sylhet sadar upazila, Appl. Geogr. 98 (June) (2018) 156–165, <https://doi.org/10.1016/j.apgeog.2018.07.012>.
- [33] I. Santé, A.M. García, D. Miranda, R. Crecente, Cellular automata models for the simulation of real-world urban processes: a review and analysis, Landsc. Urban Plann. 96 (2) (2010) 108–122.
- [34] S. Mansour, M. Al-Belushi, T. Al-Awadhi, Monitoring land use and land cover changes in the mountainous cities of Oman using GIS and CA-Markov modelling techniques, Land Use Pol. 91 (2020), 104414.
- [35] S. Ullah, K. Ahmad, R.U. Sajjad, A.M. Abbasi, A. Nazeer, A.A. Tahir, Analysis and simulation of land cover changes and their impacts on land surface temperature in a lower Himalayan region, J. Environ. Manag. 245 (February) (2019) 348–357, <https://doi.org/10.1016/j.jenvman.2019.05.063>.
- [36] S. Ullah, et al., Remote sensing-based quantification of the relationships between land use/land cover changes and surface temperature over the lower Himalayan region, Sustainability 11 (19) (2019) 5492.
- [37] A.-A. Kafy, et al., The operational role of remote sensing in assessing and predicting land use/land cover and seasonal land surface temperature using machine learning algorithms in Rajshahi, Bangladesh, Appl. Geomatics 13 (4) (2021) 793–816, <https://doi.org/10.1007/s12518-021-00390-3>.
- [38] W.-S. Lee, S.-G. Jung, The application of a prediction model on land surface temperature using Artificial Neural Network and Scenario: focused on Changwon in South Korea, J. Korea Planners Assoc. 49 (1) (2014) 263, <https://doi.org/10.17208/jkpa.2014.02.49.1.263>.
- [39] M.A. Fattah, S.R. Morshed, S.Y. Morshed, Multi-layer perceptron-Markov chain-based artificial neural network for modelling future land-specific carbon emission pattern and its influences on surface temperature, SN Appl. Sci. 3 (3) (2021) 1–22, <https://doi.org/10.1007/s42452-021-04351-8>.
- [40] A. Sekertekin, N. Arslan, M. Bilgili, Modeling diurnal land surface temperature on a local scale of an arid environment using artificial neural network (ANN) and time series of landsat-8 derived spectral indexes, J. Atmos. Sol. Terr. Phys. 206 (2020), 105328, <https://doi.org/10.1016/j.jastp.2020.105328>.
- [41] A. Satorra, P.M. Bentler, Ensuring positiveness of the scaled chi-square test statistic, Psychometrika 75 (2) (2010) 243–248.
- [42] A.A.A. Al-sharif, B. Pradhan, A novel approach for predicting the spatial patterns of urban expansion by combining the chi-squared automatic integration detection decision tree, Markov chain and cellular automata models in GIS, Geocarto Int. 30 (8) (2015) 858–881, <https://doi.org/10.1080/10106049.2014.997308>.
- [43] T. Hauschild, M. Jentschel, Comparison of maximum likelihood estimation and chi-square statistics applied to counting experiments, Nucl. Instruments Methods Phys. Res. Sect. A Accel. Spectrometers, Detect. Assoc. Equip. 457 (1–2) (2001) 384–401, [https://doi.org/10.1016/S0168-9002\(00\)00756-7](https://doi.org/10.1016/S0168-9002(00)00756-7).
- [44] F.B. Bryant, A. Satorra, Principles and practice of scaled difference chi-square testing, Struct. Equ. Model. 19 (3) (2012) 372–398, <https://doi.org/10.1080/10705511.2012.687671>.
- [45] H. Cao, J. Liu, J. Chen, J. Gao, G. Wang, W. Zhang, Spatiotemporal patterns of urban land use change in typical cities in the greater mekong subregion (GMS), Rem. Sens. 11 (7) (2019) 801.
- [46] A.A. Kafy, M.N.H. Naim, G. Subramanyam, N.U. Ahmed, A. Al Rakib, M.A. Kona, G.S. Sattar, Cellular Automata approach in dynamic modelling of land cover changes using RapidEye images in Dhaka, Bangladesh, Environmental Challenges 4 (2021), 100084.
- [47] V. Anand, B. Oinam, Future land use land cover prediction with special emphasis on urbanization and wetlands, Remote Sens. Lett. 11 (3) (2020) 225–234.
- [48] G. Fernando, Identification of urban heat islands & its relationship with vegetation cover: a case study of colombo & gampaha districts in Sri Lanka, J. Trop. For. Environ. 8 (2) (2018).
- [49] J.S. Silva, R.M. da Silva, C.A.G. Santos, Spatiotemporal impact of land use/land cover changes on urban heat islands: a case study of Paço do Lumiar, Brazil, Build. Environ. 136 (2018) 279–292.
- [50] N.N. Dey, A. Al Rakib, V. Raikwar, Geospatial modelling of changes in land use/land cover dynamics using Multi-layer perception Markov chain model in Rajshahi City, Bangladesh, Environ. Challenges 4 (May) (2021), 100148, <https://doi.org/10.1016/j.envc.2021.100148>.
- [51] A. Al Kafy, N.N. Dey, A. Al Rakib, Z.A. Rahaman, N.M.R. Nasher, A. Bhatt, Modeling the relationship between land use/land cover and land surface temperature in Dhaka, Bangladesh using CA-ANN algorithm, Environ. Challenges 4 (June) (2021), 100190, <https://doi.org/10.1016/j.envc.2021.100190>.